X-Ray Diagnostics for the Levitated Dipole Experiment

by

Jennifer L. Ellsworth
B.A., Wells College (2002)
B.S., Columbia University (2002)

Submitted to the Department of Nuclear Engineering
in partial fulfillment of the requirements for the degree of
Master of Science
at the
MASSACHUSETTS INSTITUTE OF TECHNOLOGY
September 2004

Author .....
Department of Nuclear Engineering
August 30, 2004

Certified by .....
Jay Kesner
Senior Scientist
Thesis Supervisor

Certified by .....
Darren Garnier
Research Scientist, Columbia University
Thesis Supervisor

Certified by .....
Ian Hutchinson
Chairman, Department of Nuclear Engineering
Thesis Reader

Accepted by .....
Prof. Coderre
Chairman, Department Committee on Graduate Students

X-Ray Diagnostics
for the Levitated Dipole Experiment

by

Jennifer L. Ellsworth

Submitted to the Department of Nuclear Engineering
on August 30, 2004, in partial fulfillment of the
requirements for the degree of
Master of Science

Abstract

Initial plasma experiments in the Levitated Dipole Experiment focus on producing hot electron, high beta plasmas using a supported dipole configuration. Plasmas are created using multifrequency ECRH and it is therefore expected that most of the plasma energy will be stored in the fast electrons, $T_e > 100$ keV. As a consequence, x-ray flux from bremsstrahlung emission is expected to be easily detectable. The energy spectrum of the x-ray emission below 740 keV is measured by a four channel pulse height analyzer using cadmium zinc telluride detectors. In addition, a single sodium iodide detector, which views energies up to 3 MeV, measures the intensity of the hot electron population. The electron temperature may be inferred from the x-ray energy. X-ray measurements are essential in diagnosing the effectiveness of various ECRH configurations. The design and installation of the pulse height analyzer are discussed in addition to the preliminary results from first plasma experiments.

Thesis Supervisor: Jay Kesner
Title: Senior Scientist

Thesis Supervisor: Darren Garnier
Title: Research Scientist, Columbia University

Acknowledgments

I am grateful to my research advisors, Jay Kesner and Darren Garnier. Their critiques of this thesis and of the research that is described, have been invaluable. They have consistently taken time to review designs, answer questions, and generally share with me their enthusiasm for plasma physics. I thank my thesis reader, Ian Huchinson, for reviewing this thesis and for his advice during my stay at MIT.

This work would not have been possible without the assistance of other members of the LDX group. I thank Ishtak Karim, Eugenio Ortiz, Alex Boxer, Scott Mahar, Austin Roach, Alex Hansen and Mike Mauel. I also thank Rick Lations and Don Strahan, who have taught me plumbing and provided useful technical advice.

I thank Patrick Franz and Peter Grudberg of XIA for patiently answering my many questions about the digital x-ray processor and related software. I must also thank Darren Garnier for providing the Xerxes driver on which the Handel and Mesa2X drivers are built, and Josh Stillerman for providing technical support for MDSPlus.

Finally, I thank my friends and family who have provided encouragement and counsel, Lisa Ellsworth, Matthew Ellsworth, Joan Poore, Juliana Belding, and especially Michael Hohensee.

Contents

List of Figures

List of Tables

Chapter 1

Introduction

The x-ray pulse height analyzer (PHA) is an essential diagnostic for the Levitated Dipole Experiment (LDX). Initial experiments in the LDX study hot electron plasmas with temperatures on the order of 100 keV. As a result of these hot electrons, significant x-ray flux is expected. The pulse height analyzer provides time resolved, spectral measurements of the x-ray energy along four chords in the plasma. This information is used to diagnose the hot electron population.

LDX has been designed to study high beta plasmas, stabilized by plasma compressibility and confined in a dipolar magnetic geometry. The poloidal field is supplied by an internal superconducting magnet carrying a maximum of 1.2 MA. This magnetic geometry is similar to that observed in the magnetospheres of magnetized planets [5][6][7]. The internal coil is levitated to eliminate eliminate losses to the coil supports.

During levitated operation, the dipole field lines form closed loops which provide toroidal confinement without toroidal fields [8]. During supported operation, the field lines intersect the coil supports. The magnetic geometry is then a mirror field with a mirror ratio ranging from 10 to 1000.

The LDX may be an attractive confinement concept for fusion because it is intrinsically capable of steady state operation and uses a simplified magnetic geometry without the need for interlocking coils. A levitated dipole reactor must operate with advanced fuels, D-D and D-He^3, because the 14.1 MeV neutrons produced in D-T

fusion would rapidly heat the levitated coil that generated the dipole magnetic field. Although this raises the bar for ignition, it eliminates the need for tritium breeding technologies and reduces the amount of neutron shielding required for a reactor. The LDX incorporates one high temperature superconducting magnet in the design; the Levitation Coil that will float the Floating Coil. The development of a levitated dipole reactor would require the development of high field, high temperature, superconducting magnets to serve as internal coils[9].

The purpose of the LDX is to understand the equilibrium, stability and confinement properties for plasmas created in the field of a levitated dipole [1]. This can be broken down into two major areas: the study of high beta plasmas stabilized by compressibility, and the study of magnetic shear free systems.

Conventional magnetic confinement devices such as tokamaks rely on the toroidal field for confinement and have a compressibility term which is nearly zero. These types of devices are stabilized by magnetic shear and good curvature. In contrast, the LDX magnetic geometry has purely poloidal field lines. As a result there is no magnetic shear and the plasma compressibility is non-zero. Interchange modes are predicted to be stabilized by compressibility as long as the pressure falls off more slowly than V^{γ}, where V is the flux tube volume, $\oint \frac{dl}{B}$, and $\gamma = 5/3$. For a point dipole, these conditions are satisfied for $P \propto R^{-20/3}$ [10].

The purely poloidal field has several other advantages. There is no particle drift from the flux surfaces, so the confinement properties are unaffected by neoclassical effects. In the absence of magnetic shear, particle and energy confinement are expected to be decoupled. In addition the device can operate in steady state without external current drive.

In purely two dimensional systems, all transport takes place via macroscopic flows. LDX is approximately two dimensional, so convective cell are expected to form[11]. For stable pressure profiles with 'good curvature', convective cells would transport energy down the pressure profile, whereas for 'bad curvature', they would transport energy up the pressure profile. If the pressure profiles are marginally stable with respect to interchange modes and stable with respect to all other modes, no energy

should transported by convective cells. If this condition is satisfied, then LDX will be able to operate at marginal stability without reducing the energy confinement time.

An x-ray pulse height analyzer is a plasma diagnostic that measures the energy spectrum of bremsstrahlung emission from the plasma. Bremsstrahlung, or "braking radiation", is emitted when a free electron interacts with the electric field of a charged particle [12]. For initial plasmas in LDX, electron–ion as well as electron–neutral interactions will contribute to the bremsstrahlung spectrum. X-rays are also emitted when hot electrons collide with surfaces, such as the vacuum vessel walls or the internal coil and the supports. It is necessary to shield detectors from this hard target bremsstrahlung with careful collimation to obtain electron temperature measurements from the pulse height analyzer measurements.

The simplest form of a pulse height analyzer is an x-ray detector that produces a charge proportional to the energy of the incident x-ray. The charge is then converted to a voltage by a charge sensitive preamplifier. Each voltage pulse is then processed and counted (or rejected). The result is an energy spectrum of x-rays incident on the detector. LDX uses a four-channel digital x-ray processor for pulse processing, described in detail in Chapter 3.

The pulse height analyzer for LDX views four chords along the midplane of the vacuum vessel, providing enough spatial resolution for qualitative profile measurements. The diagnostic relies on 5x5x5 mm CZT (cadmium zinc telluride) detectors with energy sensitivities of 10 keV to 670 keV. Additional measurements can be made at higher energies using a 2x2" NaI (sodium iodide) scintillation detector, capable of measuring x-rays with energies as high as 3 MeV. The CZT detectors were selected for their small size and superior energy resolution.

Time resolution is achieved by measuring multiple spectra during the course of a shot. Sixty-four spectra can be stored at the maximum resolution of 8184 bins. The time windows during which the spectra are recorded can be individually varied. Additional spectra can be measured before and after each shot.

For initial plasmas, the output of a sodium iodide detector, positioned to look directly at the F-coil, was amplified and digitized. These x-ray emission measurements

may provide some insight about the conditions that produce the most hot electrons. For example, puffing gas into the plasma during the shot may affect the x-ray signal. Similarly, changing the timing of the two RF frequencies will vary the pressure profile which will change the x-ray emission profile, and may affect the stability of the plasma as well.

When the velocity distribution of the hot electrons is maxwellian, then $I/E = N(E) = \exp(E/T)$, where N is the number of counts for a given energy, I is the x-ray intensity in arbitrary units and T is the hot electron temperature. Neglecting corrections, the temperature is the inverse slope of a straight line fit to a log–linear plot of counts versus energy. Assuming there is little variation in the plasma in the field of view of the detector, and that Z_{eff} is close to one, the bremsstrahlung power is proportional to $n_{ehot} n\sqrt{T}$. The bulk density of the plasma is measured by the interferometer so the hot electron density can now be computed. A qualitative picture of how the hot electron population is distributed within the plasma and how that distribution evolves over time can be obtained. This kinetic pressure profile can be compared to the pressure profiles reconstructed from magnetics measurements using the Grad-Shafranov equation.

The goals for the pulse height analyzer are to look at hot electron plasmas with high beta to get an idea of the pressure profile kinetically. We would like qualitative measurements of the kinetic pressure profile to determine if the theoretical conditions for stability are met. We may be able to set some benchmarks for how plasmas behave in different magnetic field configurations.

We would also like to investigate the x-ray spectrum to determine the maximum energy, and number of x-rays emitted. This will indicate how efficient the hot electron production is, whether there are any preferential hot electron losses at some energies and the upper limit of the electron energies, indicating microinstabilities like the mirror instability.

The purpose of this thesis is to design, calibrate, and test the x-ray diagnostics for the LDX and to use measurements from these diagnostics to analyze the ECRH heating of first plasmas.

Chapter Two highlights important details of the Levitated Dipole experiment, including the magnetic geometry, initial diagnostic set, and predictedl plasma parameters. The pulse height analyzer detectors were calibrated using an Am-241 source which has a calibration line in the range of the expected x-ray emission from LDX plasmas. The details of the x-ray pulse height analyzer including the choice of detectors, collimation, the data acquisition system and calibration are described in Chapter Three. The last chapter will present the results of initial experiments in LDX.

Chapter 2

The Levitated Dipole Experiment

Plasma confinement in dipolar magnetic fields is studied in the Levitated Dipole Experiment (LDX). In nature, this configuration has been observed to confine the plasmas surrounding neutron stars and the middle magnetospheres of planets such as Jupiter and Earth [5].

The idea of using a dipole field for a fusion reactor was developed by Akira Hasegawa after the Voyager II spacecraft detected plasma trapped in the magnetic field of Jupiter's magnetosphere [6]. Hasegawa observed that global fluctuations in laboratory plasmas resulted in rapid plasma and energy loss, while in planetary magnetospheres, strong electromagnetic fluctuations result in inward diffusion and heating. He proposed that a dipole reactor operating with marginally stable pressure profiles, similar to those found in nature, might not exhibit anomalous transport.

Previous experiments have studied the behavior of plasmas confined by multipole fields in multipoles, spherators, and terrella experiments. Terrella experiments have explored magnetospheric physics. Among these are the Princeton Levitated Spherator-FM1[13], the Wisconson Toroidal Octupole Experiment[14], the Culham Levitron [15], and the Birkeland Terrella Experiment in Finland. While spherators, which require complicated interlocking coils, the LDX uses a ring coil. The LDX magnets produce significantly more magnetic flux that previous multipole experiments, so pressure profiles of marginal stability can be investigated. In addition, a larger vacuum vessel will allow us to study flux expansion.

Several dipole geometry experiments are currently underway worldwide. The collisionless terrella experiment (CTX) is investigating supported dipoles [16]. The LDX will operate at higher field than CTX and will be capable of levitated operation. Mini–RT in Japan is studying cold, single species plasmas with a 6 cm diameter levitated dipole. The LDX, in contrast, has a 68 cm diameter floating coil, and will initially study hot electron (neutral) plasmas. The levitated coil is expected to improve confinement properties as compared to supported dipole experiments in which particles are lost to the coil supports; this is similar end losses in mirror machines.

This chapter will present a brief overview of the experiment, including the magnetic geometry, heating and diagnostic set.

2.1 Magnetic geometry

The magnetic geometry of LDX is achieved using three superconducting magnets. The dipole magnetic field is provided by an internal Floating coil (F-coil) carrying 1.2 MA. During floating operation, the 550 kg F-coil will be continuously levitated from above using the levitation coil (or L-coil). In supported mode, the L-coil may also be used to provide some plasma shaping. The F-coil is inductively charged by a 3.2 MA charging coil (C-coil). Fig. 2-1 shows a cutaway view of LDX with the three magnets and the field lines for levitated mode with the L-coil at full field. Additional plasma shaping can be achieved by imposing a vertical magnetic field with two copper Helmholtz coils.

Initial plasmas in LDX use a supported dipole configuration. The F-coil is energized to 60% of the full current, 0.75 MA. Equilibrium field lines without shaping are show in figure 2-2.

2.2 Plasmas

LDX plasmas will typically be hydrogenic. Initial experiments were performed using deuterium gas as fuel. Hydrogen, helium and argon are also available for experiments

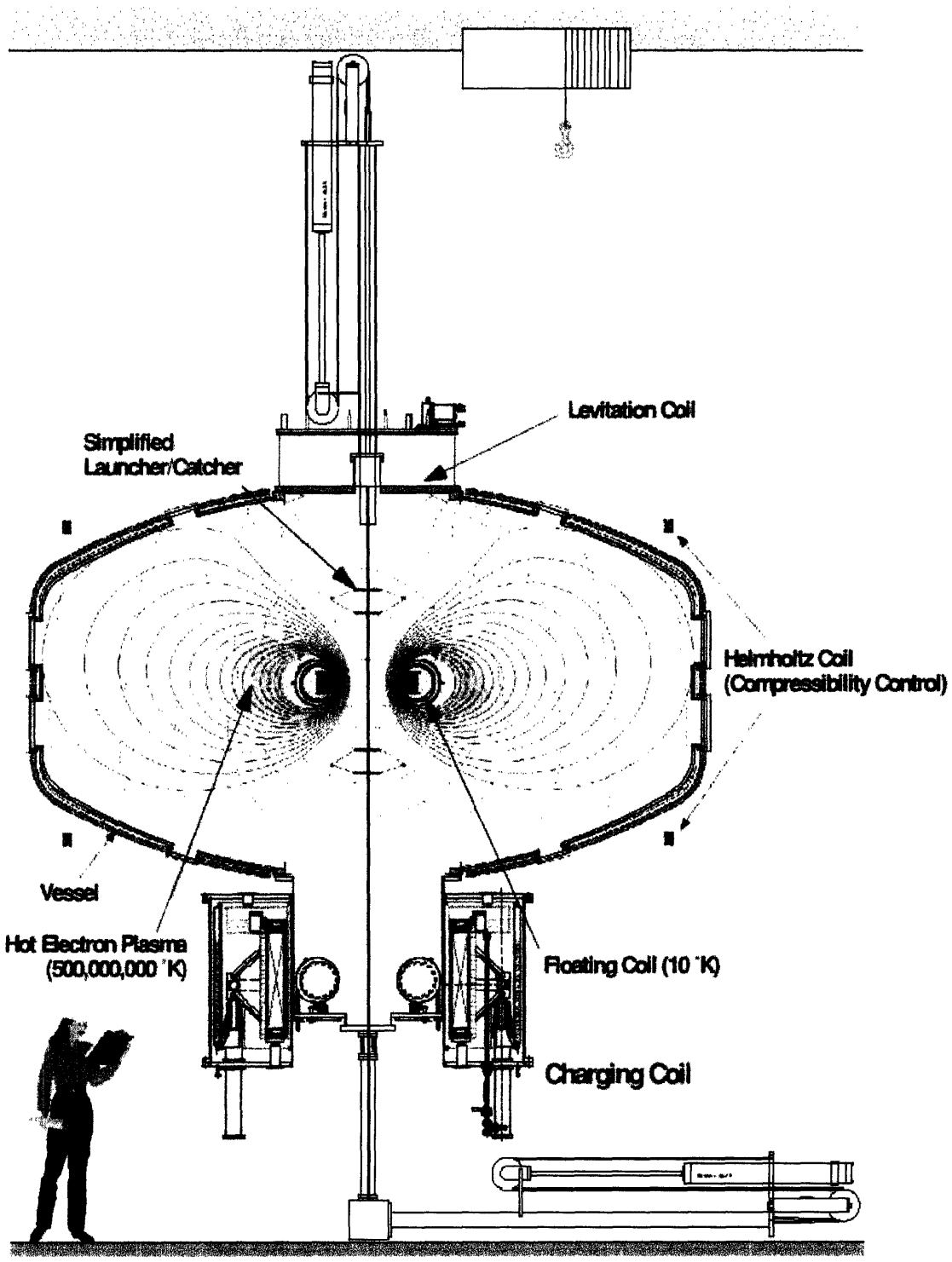

Figure 2-1: A cross section of the LDX experiment is shown with the basic coil configuration. Magnetic field lines (solid) and $|B|$ contours (dotted) are drawn for the plasma equilibrium resulting for levitated operation [1].

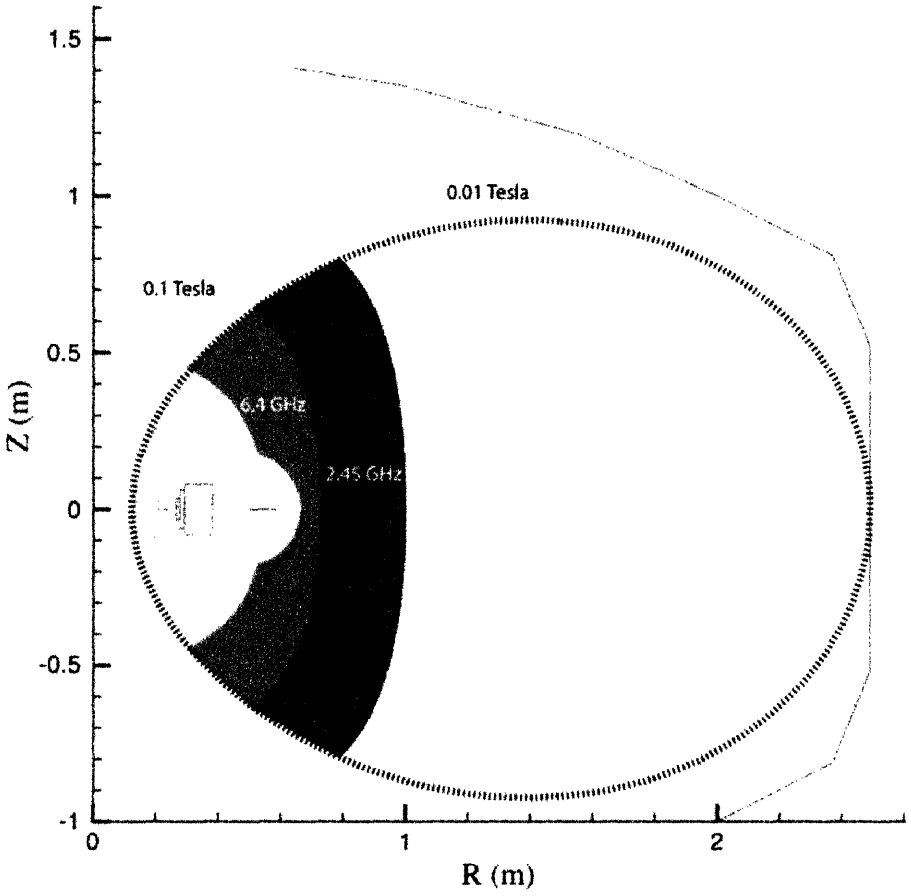

Figure 2-2: Typical magnetic geometry for first plasmas. Pressure contours are indicated by solid lines and magnetic field contours with dashed lines. The hashed line is the last closed flux surface. 2.45 GHz and 6.4 GHz resonance heating zones are shown within the labeled regions. The outer band of each region is the cold plasma resonance, while the inner band is the resonance for 200 keV electrons [2].

on mass or charge scalings. Argon plasmas may be used to enhance x-ray signals by virtue of their high atomic number, Z, as bremsstrahlung power increases with increasing atomic number.

Initial plasmas are created using multifrequency electron cyclotron resonance heating (ECRH) at 2.45 GHz and 6.4 GHz. Each RF source will produce 3 kW of power. In addition, higher power 10 GHz, 18 GHz, and 28 GHz sources will be incorporated in future run campaigns. Particle orbits are closed so hot electrons should be well confined. As a result, these electrons heated by ECRH should reach high temperatures, on the order of 100 keV. In order to reach these temperatures using the configuration for first plasmas, shots on the order of ten seconds may be required.

The resonance zones for initial plasma experiments without shaping are shown in Fig. 2-2. The outermost line of each zone, 140 Gauss and 370 Gauss for 2.45 GHz and 6.4 GHz, respectively, are the cold plasma resonances for each frequency. As the electrons become relativistic, their lab frame mass increases and the resonance shifts inward. The inner edge of the resonance zone pictured is the second harmonic for electrons with $\gamma = \sqrt{(1/(1 - v^2/c^2))} = 1.4$. The hashed line marks the last closed flux surface. The edge of the vacuum vessel is also show. The F-coil is pictured in the center of the field lines.

There are two 'knobs' on the initial experiments. We turn the first by adjusting the power of the ECRH sources. This should adjust the height of the plasma profile. We are also able to vary the relative power of the two sources, which may shift the location of the pressure peak. Our second control is the gas pressure. Initial experiments include a gas puff scan, during which deuterium gas is puffed into the vessel in varying amounts.

An additional knob will be used in the future. The shape of the plasma can be manipulated by applying a vertical magnetic field via the Hemholtz coils or by energizing the L-coil with a small amount of current. Plasmas can be shaped to a limited mode or a diverted mode.

The initial plasmas discussed in this thesis use a supported dipole configuration with no shaping. The F-coil current is 40% of the design current, approximately

0.6 MA so the maximum poloidal magnetic field is 0.022 Tesla. Plasma density is predicted to be a maximum of $10^{17}m^{-3}$. Maximum edge densities are expected to be in the range of 10^{16} m^{-3}. Hot electron electrons were observed in the range of 20 keV to 150 keV. The bulk ion and electron populations are expected to have temperatures in the low eV range.

Estimates of predicted plasma parameters for plasmas created using the F-coil at full field with no shaping, limited mode, and diverted mode are given in Table 2.1 for four configurations. These parameters are for plasmas in levitated mode. Plasma densities in the range of 10^{17} to $5 * 10^{18}$ m^{-3} are expected.

Table 2.1: Plasma equilibria parameters. (A) diverted, no shaping, (B) diverted, shaped for maximum beta, (C) diverted, shaped for minimum beta, (D) limited plasma [1].

	A	B	C	D
S-Coil Currents; I_{s1}, I_{s2} (kA)	0,0	1,12	50,50	3,12
Plasma Volume (m^3)	14	27	1.7	24
SOL Pressure (Pa)	0.25	0.25	0.25	0.1
Max Pressure (Pa)	1.35	1530	45	472
Plasma Current(kA)	3.2	16.4	0.39	5.78
Stored Energy (J)	315	1450	27	516
R(P_{max}) (m)	0.76	0.76	0.77	0.79
B(P_{max}) (T)	0.088	0.088	0.088	0.088
$\beta(P_{max})$	0.08	0.55	0.015	0.15

2.3 Diagnostic set

In addition to the x-ray pulse height analyzer, the initial diagnostic set includes measurements of the pressure profile, plasma core density, edge density, x-ray intensity and electron temperature. Two black and white CCD cameras provide side and top views of the visible radiation and the launcher/catcher and positioning of the F-coil. A color, digital video camera views from the side of the vessel. The locations of the initial diagnostics on the vacuum vessel are shown in Fig. 2-3.

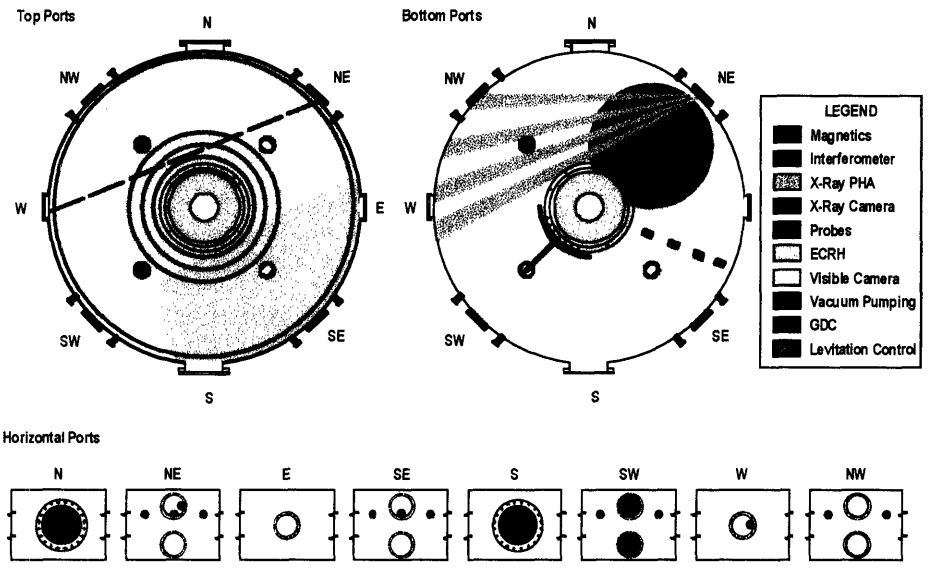

Figure 2-3: Placement of initial diagnostic set on LDX [3].

External magnetic measurements include eighteen poloidal field coils spaced poloidally on the vacuum vessel at a fixed toroidal location. Six flux loops measure the flux along the z-axis. These measurements can be used to reconstruct the MHD equilibrium pressure profiles. These measurements are digitized at a rate of 200 kHz.

Internal magnetics will look at magnetic fluctuations potentially caused by interchange modes. One internal Mirnov coil will measure the magnetic fluctuations of first plasmas. The coils are capable of temporal resolution as high as several MHz. Seven additional Mirnov coils and three additional flux loops are available for installation at a later date.

Three fixed position Langmuir probes measure edge density fluctuations at a position 12 cm from the wall of the vacuum vessel. A Mach probe, protruding 60 cm into the vessel, measures the differences in ion velocities, from which plasma flows can be detemined. A one-channel heterodyne interferometer operating at a frequency of 60 GHz will measure the core plasma density. Additional channels will be installed after the prototype is tested. This measurement was not digitized for initial experiments, but estimates based on observation of fringes on the oscilloscope are available.

A 2x2" NaI detector views the center of the vacuum vessel. This channel provides a

measurement of the intensity of x-ray emission from the plasma at 30 kHz bandwidth. This intensity can then be used to classify plasmas.

Chapter 3

Experimental Apparatus: Pulse Height Analyzer Description

For LDX plasmas, bremsstrahlung emission is expected from interactions between free electrons and free ions, as well as interactions between free electrons and neutral particles. Bremsstrahlung is also emitted when hot electrons collide with objects in the vacuum vessel, namely the F-coil, the F-coil supports, and the chamber walls. The energy spectrum of this x-ray emission is measured with a four channel pulse height analyzer. The design, installation and calibration of this diagnostic are described in the following chapter.

3.1 Pulse Height Analyzer Design Requirements

Equilibrium pressure profiles were computed using the dipoleq code[10]. The code computes a free boundary solution to the Grad-Shafranov equation by iteratively updating the boundary conditions from Green's functions and then solving the Grad-Shafranov equation on a fixed grid. The pressure profiles of interest are those that produce the highest values of beta. For fixed edge pressures, beta is maximized for pressure profiles that are marginally stable to interchange modes. The location of the pressure peak is specified, and the pressure is set to zero at the surface of the Floating Coil and at the last closed flux surface (or the vacuum vessel wall if it is

closer). Between the coil and the pressure peak, the pressure is varied cosinusoidally, $P(\psi) = 0.5(1 - \cos[\pi(\phi - \phi_0)/(\phi_{peak} - \phi_0])$, whereas between the pressure peak and the last closed flux surface, the pressure falls off as $P \propto 1/V^{\gamma}$.

Maximum values for peak density are fixed by the frequency of the ECRH. Multi-frequency ECRH at 2.45 GHz and 6.4 GHz are installed for initial experiments, with higher frequencies scheduled for installation at later dates. At these frequencies, peak densities of roughly half the cutoff frequency are typical; 10^{18} cm^{-3} is expected. The MHD equilibria do not specify the relationship between density and temperature, so we rely on kinetic theory to choose η, where $\eta = d\ln T/d\ln n$. The value, $\eta = 2/3$, was selected because it is predicted to be most stable to the flute–like drift frequency instability known as entropy mode[17]. Most of the energy in the plasma is stored in the hot electrons, so the bulk electron and ion temperatures are assumed to be negligible for the purposes of this calculation. The magnetic field, beta, and the relative pressure are plotted in Fig. 3-1 for an equilibrium assuming maximum beta of 0.562 and pressure peak location of $r = 0.848$ m, as measured from the center for of the vacuum vessel.

The bremsstrahlung emission from the plasma is then computed by summing $\frac{dP_b}{dV}dV$, where

$$dP_b/dV = 1.6910^{-32} n_{eh} n_i \sqrt{T},$$

P_b is the power due to bremsstrahlung emission , V is the plasma volume, and we have assumed $Z_{eff} = 1$. Estimated values of bremsstrahlung power are plotted in Fig.3-1. The count rate on a detector can be computed by taking the total power incident on the the detector surface and dividing by the average energy of the incident x-rays as described in section 3.2.5.

For more accurate predictions, special relativity should be taken into account. These predictions are, however, sufficient for our purposes: estimating the broad range of operating parameters for the PHA.s

The pulse height analyzer system for LDX has nominal design values of 100 keV hot electron temperature and 10^8 cps. This assumes 3 W of bremsstrahlung power,

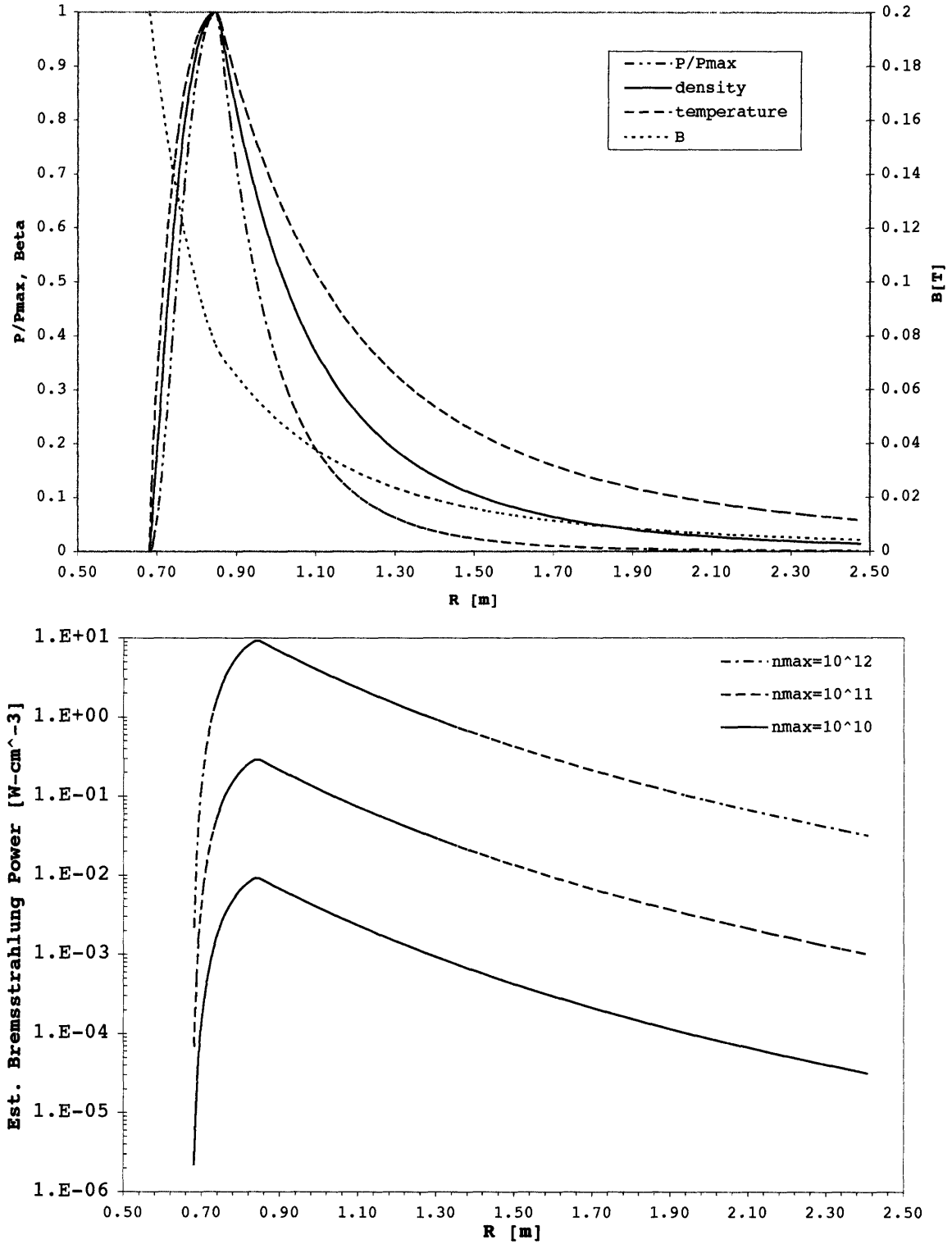

Figure 3-1: Top: Predicted pressure, beta, and magnetic field profiles generated from equilibrium reconstruction code. Bottom: Corresponding bremsstrahlung emission profiles assuming $P = n_{ehot}T_{ehot}$ for densities of $n = 10^{16}cm^{-3}$, $n = 10^{17}cm^{-3}$, and $n = 10^{18}cm^{-3}$.

which is an intermediate value between the total estimated power emitted for peak densities of $10^{10}cm^{-3}$ and $10^{11}cm^{-3}$. Ideally, the temporal resolution should be on the order of the energy confinement time, but it must be long enough that a sufficient number of counts are collected for statistical analysis. Detectors and preamplifiers must be able to operate in 500 Gauss magnetic field.

3.2 Pulse Height Analyzer Layout

In its simplest form, a pulse height analyzer is a detector which outputs a charge proportional to the energy of an incident x-ray. A charge sensitive preamplifier converts the charge to a voltage pulse which is then filtered, and counted. Traditionally, pulse height analyzers have used analog electronics for pulse processing. In contrast, we've chosen to use a multichannel analyzer card, the Digital X-Ray Processor, DXP model 4C2X from X-Ray Instrumentation Associates (XIA), which runs on the CAMAC standard. In this device, the preamplifier signal is digitized, while the pulse height determination, filtering, and spectrum binning are all done using digital electronics. The chief advantage to LDX of a digital system compared to an analog system is the higher throughput it affords. Analog filtered pulses can have tails lasting as long as 40% of the peaking time, unlike the sharp termination of the digital filter. The DXP can handle count rates up to 500 kcps.

3.2.1 Detectors/preamplifiers

Typical detector materials include silicon, sodium iodide (NaI), mercuric iodide, cadmium telluride (CdT), cadmium zinc telluride (CZT). The type of detector chosen for each application depends on a number of considerations including the resolution, energy range, maximum count rate, and cost. Better resolution can be obtained by cooling detectors. Indeed, silicon detectors require cooling to liquid nitrogen temperatures. The CZT detectors chosen for the LDX pulse height analyzer function well at room temperature.

There are two types of charge sensitive preamplifiers: reset preamplifiers and RC

feedback preamplifiers. In a reset preamplifier, the output voltage is reset to zero between pulses. These are more difficult to build than feedback preamplifiers and are therefore more costly. During the reset there is a short 'dead time' during which no data can be collected. This type of preamplifier tends to be used with detectors for experiments that view soft x-rays and require high accuracy. An RC feedback preamplifier is an RC circuit, thus the output voltage decays exponentially with time constant $\tau = RC$. Features are added to reduce noise and to correct for undershooting, which is a transient effect following a pulse. RC feedback preamplifiers are comparatively inexpensive, but are noisier than reset preamplifiers. RC feedback preamplifiers are used in the LDX system as the resolution provided by reset preamplifiers would be superfluous and RC feedback preamplifiers are more readily available for high energy x-ray detectors.

Off the shelf detector and preamplifier units are available and adequate for our purposes. These units are fairly inexpensive and don't require time consuming development. Two types of detectors are available for our experiments, CZT detectors and NaI detectors. A summary of the detector and preamplifier properties for both the CZT and NaI detector assemblies can be found in Table 3.1 and a photograph is shown in Fig. 3-2. The sensitivity of the preamplifier is given in mV/keV. The average step size indicates the voltage output caused by a 100 keV x-ray. The rise time is the time it takes the voltage to spike after the arrival of an x-ray photon and the fall time, is the RC decay time of the preamplifier circuit, τ_{RC}. The noise equivalent charge is the charge that would be produced in a silicon detector due to the noise in the detector of interest.

We use four CZT 5x5x5 mm crystal SPEAR detectors from eV Products. These units are packaged with built in preamplifiers. The window is 0.001" aluminum, and the detector has a gold shield. The detector is shielded from visible light, but additional shielding from UV radiation is necessary. The resolution is 4% full width half max (FWHM) at 122 keV. The preamplifier has a rise time of 35 ns at the source and a fall time of 750 μs. These detectors require a bias voltage from 500 V to

Table 3.1: Comparison of the characteristics of the Bicron 1378 NaI detector to the eV Products SPEAR CZT detector.

Parameter	NaI	CZT
Type	RC feedback	RC feedback
Energy Range	15 keV - 3 MeV	10 keV - 670 keV
Resolution	10% FWHM 662 keV	4% FWHM 122 keV
Output gain	0.6 mV/keV	0.11 mV/keV
Rise Time	0.2 μs	0.035 μs
Decay time	50 μs	725 μs
Noise Equiv. Charge	160 e^- @ Cin = 6pF	160 e^- for Ce source
Ave Step Size	60 mV	11 mV
Assembly dimensions	2.31 " x 7.94"	12 mm x 89 mm

Figure 3-2: Photographs of the NaI and CZT detectors used to measure x-ray emission from LDX plasmas.

1000 V and the preamplifier requires a 12 V power supply. The Spear CZT detector can function in static magnetic fields up to 5 Tesla, although time varying magnetic fields may interfere with the operation of the preamplifier. Careful alignment, or magnetic shielding may be required for experiments in levitated mode.

We use one NaI detector, model IA–1378 from Bicron[18]. This detector uses a thin (1 mm) NaI crystal, 50.8 mm diameter and an aluminum entrance window. The detector is optically coupled to a photomultiplier tube that is terminated by a 14–pin phenolic base. The photomultiplier tube and detector are shielded from external visible light by a mu–metal magnetic shield. Its resolution is 8% full width half max for Cs–137 at 662 keV.

The NaI detector is used in conjunction with an Ortec model 296 photomultiplier tube base and high voltage power supply. The bias voltage of the high voltage power supply is adjustable from 600 V to 1100 V, and is powered at 12 V in turn by a low ripple detector power supply. This power supply is used to run all x-ray detectors on LDX. The Ortec 296 incorporates a preamplifier which has as risetime of 100 ns at the source and the nominal fall time is 50 μs. Observed fall times in the LDX setup are 90 μs on average. The sensitivity is user selectable, either 1 μV/keV (LDX selection) or 6 μV/keV. The spectral broadening is quoted as 10% at 662 keV. This sets the resolution for the detector/preamplifier pair as the detector resolution is 8% for the same line.

The NaI detector has a larger energy range than the CZT detectors, 15 keV – 3 MeV compared to 10 keV – 670 keV whereas the CZT detector has better resolution than the NaI detector, 4% full width half max at 122 keV versus 10% full width half max at 662 keV. The CZT detectors are also much smaller in size than the NaI detectors.

The digitizer has only four channels so at most four of the five detectors may be used simultaneously for pulse height analysis. Most of the emission is expected to be within the range of the CZT detectors (10 keV – 670 keV) [19]. Experiments from the collisionless terella experiment (CTX) at Columbia University occasionally see x-ray emission at energies as high as several MeV[20] so the NaI detector will measure the

overall x-ray emission from the LDX experiment. We can then be be sure we are not ignoring a high energy tail.

The smaller surface area of the CZT detector is not expected to be a problem in the long run, although initial experiments using a reduced F-coil field will produce less x-ray flux than later experiments with full field and optimized plasma control. With an area of 25 mm^2, 8 Mcps are expected with no collimation. Although the CZT is detector is much smaller than NaI detector, it is 50% more dense than NaI so has better count rate per unit volume.

The detector unit was chosen based on the properties of the preamplifier. Because we expect a high count rate, we require a preamplifier with a fast rise time. The predicted count rate, gain and fall time are used to determine the voltage range of the output of the detector. The output must fall within the voltage range of the digitizer for the DXP (0–10 V). Ideally, we want to use as much of this range as possible without exceeding the maximum in order to increase our signal to noise ratio.

The change in preamplifier output voltage due a beam of mono-energetic x-rays, with energy E_{ave}, striking the detector at a constant rate, dN/dt, is given in Eq. 3.1. Here, N is the number of incident x-rays, G is the preamplifier sensitivity, and τ_{RC} is the fall time.

$$\frac{dV}{dt} = GE_{ave}\frac{dN}{dt} - \frac{V}{\tau_{RC}} \tag{3.1}$$

The first term is the product of the voltage increase due to an incident x-ray and rate at which these steps occur, which gives us the voltage increase resulting from the beam. The second term is the exponential decay of the voltage resulting from the RC circuit. The maximum output voltage is then,

$$V_{max} = GE_{ave}\frac{dN}{dt}\tau_{RC}. \tag{3.2}$$

Using Eq. 3.2, a maximum voltage of 4.0 V was computed for the CZT detector, assuming an average x-ray energy of 100 keV, detector sensitivity of 0.11 mV/keV, and fall time of 725 μs. Although the built in RC feedback preamplifier in the Spear

detector can handle count rates up to 550 kcps, the pulse height analysis electronics are limited to 500 kcps, and so this value was used as dN/dt. 4.0 V is within the accepted range of the DXP. The DC offset of the Spear detector is less than 100 mV so this will not affect the result significantly. The NaI detector has a gain of 0.6 mV/keV and a decay time of 50μs so the maximum voltage assuming 500 kcps is 1.5 V.

3.2.2 Views and collimation

The chords that the pulse height analyzer will view were chosen such that the entire midplane of the plasma would be sampled. Because we would like to investigate how varying the plasma heating affects the pressure peak, the chords were chosen to be equidistant in angle, rather than clustered where the pressure peak is expected. We would also like to have the flexibility to diagnose plasmas that do not behave as expected. Fig. 3-3 illustrates the detector views in the LDX vacuum vessel.

The collimator is designed for four CZT detector assemblies with 12 mm diameter. The collimator features an adjustable viewing angle and a replaceable pinhole. The entire assembly is designed to be flexible in the amount of collimation provided so that the pulse height analyzer can be easily adapted to a wide variety of plasma conditions. In the event that the bremsstrahlung emission is weaker than expected, the collimation angle can be increased to allow for more signal. The design angle of four degrees was selected so that a full view of the plasma midplane could be obtained. The collimator is made of lead, and the shortest thickness through which an unwanted photon must pass to reach a detector is 1 inch.

A pinhole was not used for first plasma operations because the x-ray flux was expected to be low in comparison to the values of x-ray flux predicted for levitated operation. The collimation is then due to a single aperture, as pictured in Fig. 3-5.

For a uniform plasma source, the signal reaching the detector is proportional to the product of the total signal emitted from the plasma and the étendue, G, defined as

$$G = A\Omega_s,$$

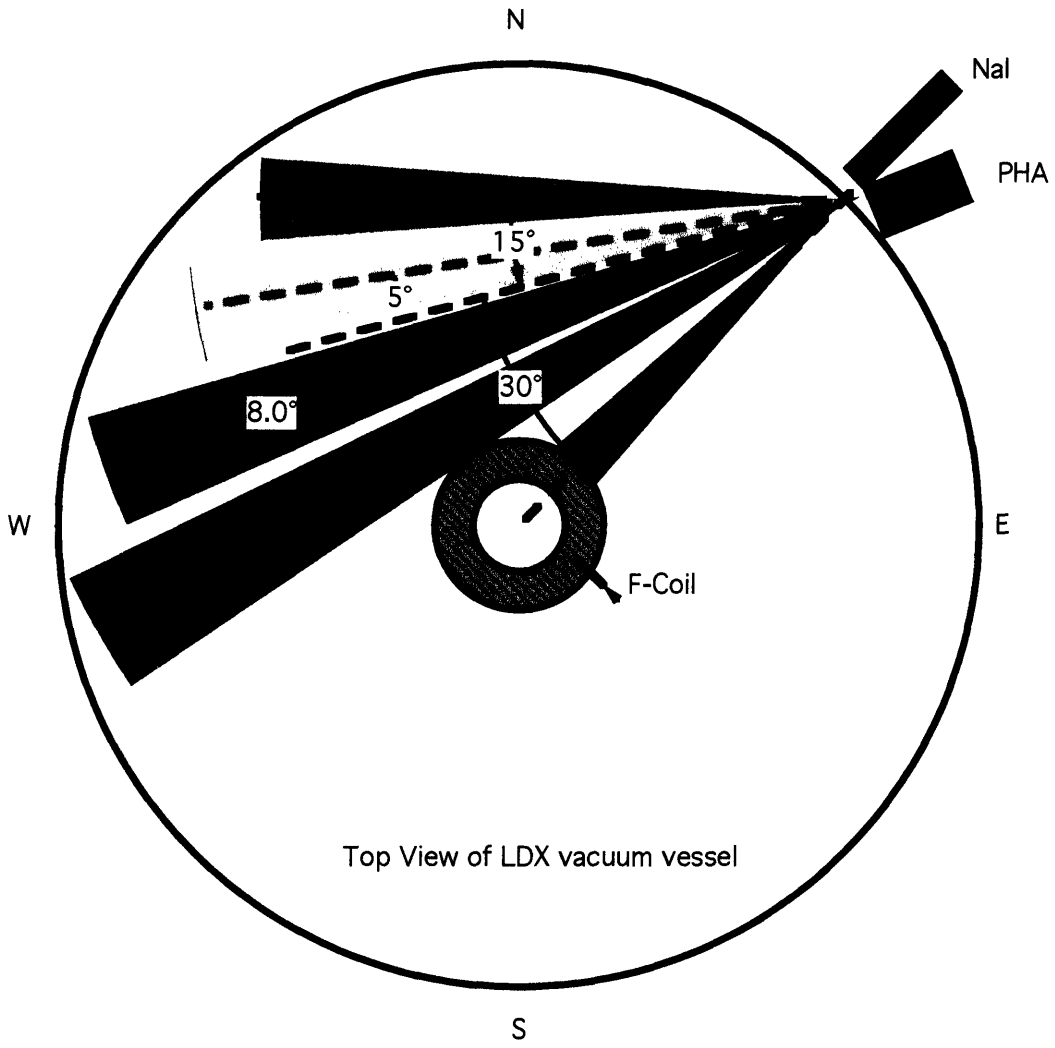

Figure 3-3: The chordal views of the Bremsstrahlung signal are shown overlayed on a cross-section of the LDX vacuum chamber. The floating coil is shown to scale in the center. An additional sodium iodide detector views directly across the vacuum vessel. The pressure peak is expected to lie close to the outer edge of the floating coil.

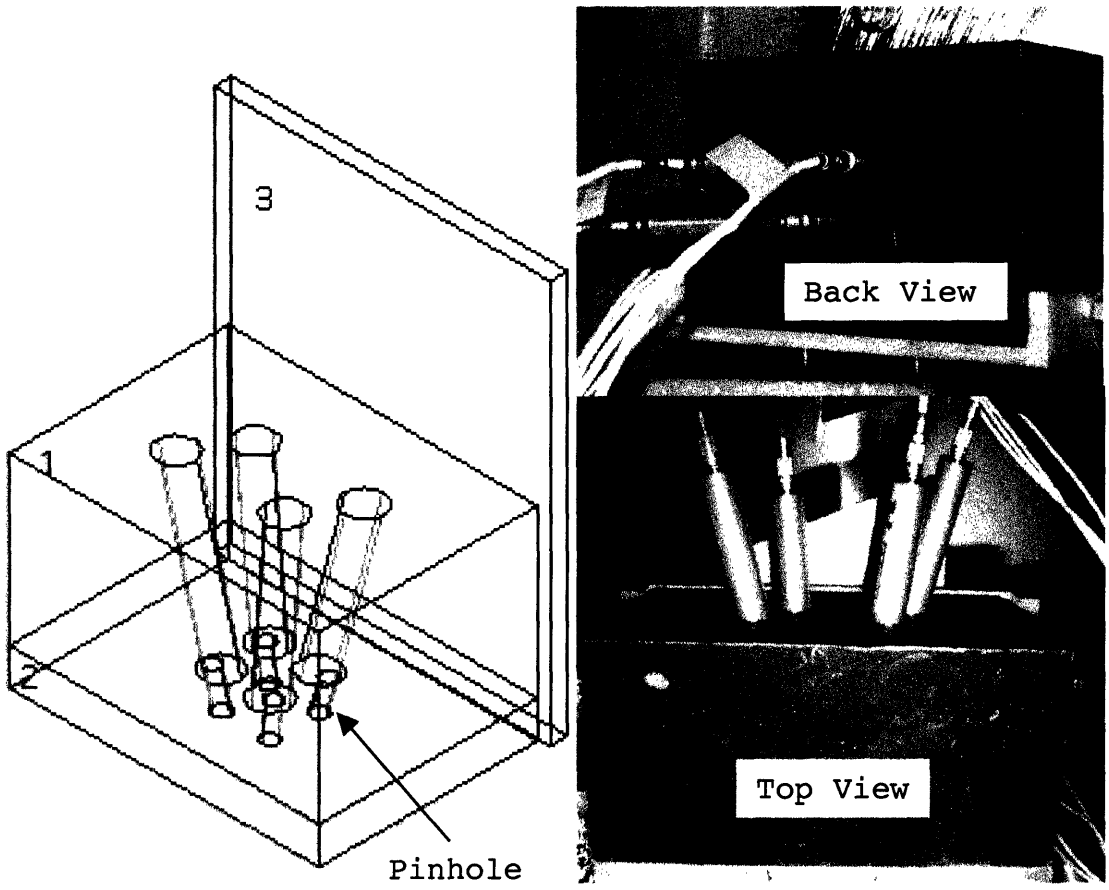

Figure 3-4: A schematic of the collimation device is shown on the left. A photograph is shown on the right.

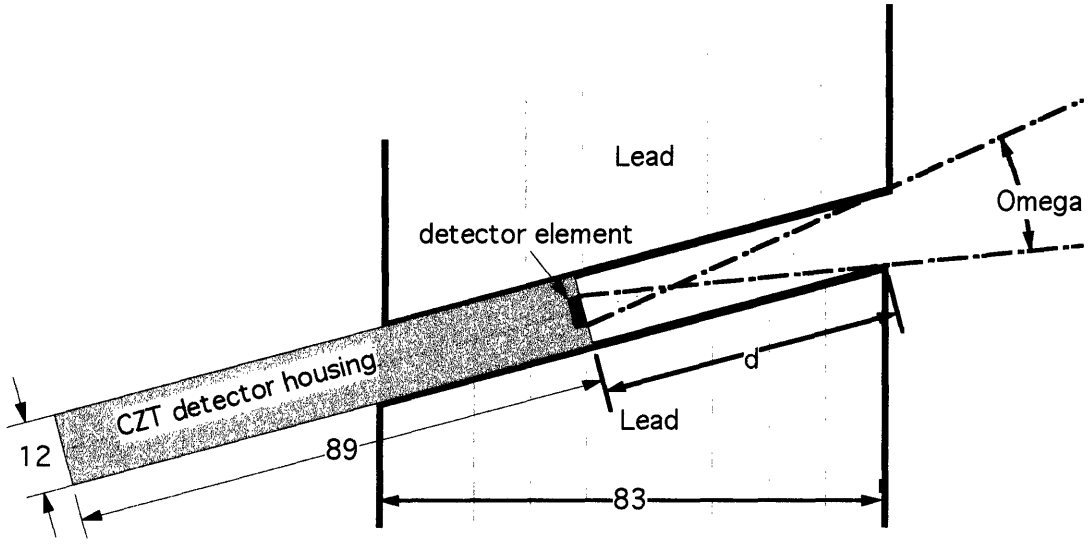

Figure 3-5: The collimation setup for first plasmas. Each CZT detector was placed in a collimation hole. Adjusting the position of the detector changes the collimation angle.

where A is the area of the detector and Ω_s is the solid angle of the of the collimating optics. When several optics are coupled together, the étendue is determined from the component with the smallest value. When a pinhole is added to the pulse height analyzer, the pinhole diameter will determine the étendue of the system. For the experiments described here, the entrance hole to the collimator defines the étendue.

We assume that the distance between the detector and the aperture, d, is much larger than the diameter of the circular bore through the lead. The aperture can then be approximated as circular, although the actual aperture is elliptical because the bore is drilled at an angle through the lead brick. In this case, the solid angle is given by $\Omega_s = A/r^2$, where A is the area subtended by the view on a sphere of radius, r. For a circular bore with diameter, w and a distance d between the detector and the aperture, the solid angle is $\pi(w/2)^2/d^2$. Typical values for first experiments are detector area of 25 mm, aperture width, w, of 12.3 mm, and a separation distance, d, of 40 mm. These produce an étendue of 1.9 mm^2-steradians.

3.2.3 Data Acquisition

Digital pulse height analysis has several advantages over the analog electronics that have traditionally been used for shaping, filtering and counting of incident pulses. The input pulse is already digitized when it reached the filters, so filtering and binning can be done during the time of the pulse, thus reducing dead time and allowing for higher count rates. In addition, digital filters have a sharp termination which increases the throughput of the system, allowing for measurement of higher count rates.

XIA Digital X-Ray Processor

The DXP can considered in four functional blocks. The analog signal conditioner (ASC) prepares the preamplifier output to be digitized. A 40 MHz analog to digital converter digitizes the output of the ASC. The FIPPI (filter, pulse detector and pile-up inspector) discriminates pulses. The digital signal processor (DSP) bins the pulses, collects statistical information about the run, and controls the other three sections.

The system components that must be understood to operate the LDX system are described in this section. The FIPPI and DSP are discussed first. These require user input parameters. The spectra and statistics that are read out of the DXP are then described. Finally, the sources of noise in the measurement are discussed.

Shaping the preamplifier output may be thought of as filtering. The DXP uses two digital filters to discriminate pulses, a fast filter and a slow filter. The purpose of the fast filter is to detect the arrival of x-rays and to prevent fast pileup, while the purpose of the slow filter is improve the energy resolution. These filters, which produce trapezoidal pulses, have a fixed length which is chosen by the user according to the properties of the preamplifier. Additional information about how filtering parameters were chosen for LDX is contained in Appendix A. The throughput of the system scales like the $1/\tau_{ps}$, where τ_{ps} is the slow filter time.

The DSP bins the data that satisfies the pile up criteria in the FIPPI. The user may select the number of bins in each spectra and the energy width of the bins. Time resolution is achieved by collecting multiple spectra during each run, termed multi-MCA mode. The number of spectra that may be recorded is limited by the maximum memory per channel, 1 MB. We have chosen to use maximum number of spectra that can be collected with the maximum number of bins, 64 spectra of 8184 bins each. Statistics are collected for each run. The time during which each spectra is collected is fixed by applying an external gate signal to the DXP.

To take advantage of this multi-MCA mode, a firmware upgrade was required for the DXP. XIA developed and tested this firmware. The LDX will be the first to put this firmware to use.

The statistics measured for each run include the realtime, livetime, input count rate and output count rate. The realtime is the total time that passed during the run. For the LDX system, the realtime should be the time during which the external gate signal was high. The livetime is the time during which the DXP actually processed events, as opposed to maintenance operations such as statistics and baseline measurements, or ASC parameter readjustments. The input count rate is the average rate at which events triggered the FIPPI. The FIPPI is triggered for each voltage pulse from

the preamplifier that is larger than a user defined threshold value. The output count rate is the average rate of counts that satisfied the criteria in the pulse pile-up criteria in the FIPPI. A dramatic difference between the input and output count rates may indicate significant pulse pile-up, or it may indicate that the threshold value is too low.

A baseline measurement is taken by periodically sampling the voltage when there are no events to process, see Fig. 3-7. The baseline should be gaussian distributed with a standard deviation that reflects the noise in the system. The height of each pulse is measured with respect to the baseline mean. Significant deviations from gaussian shaped baselines may indicate systemic noise in the system. If the mean position of the baseline is not zero, the height of the input pulses are scaled using the baseline mean as zero. This introduces some statistical noise into the measurement, $(1/8)\sigma_e$.

Electronic noise in the system is introduced by fluctuations in the power supplies, capacitance in the cabling and frequency sources in the surrounding area. The standard deviation of this electronic noise, σ_e, is typically less than 0.5 mV in the LDX system. Additional noise is introduced by the leakage current from the detector. This fano noise, σ_f, is given in terms of the number of electrons that would be emitted from a silicon detector with an equivalent noise level. For CZT detectors, the noise equivalent charge in silicon is 160 electrons. The pair creation energy in silicon is 3.63 eV so the noise level due to leakage current is approximately 0.063 mV at the output of the preamplifier. The total noise sums in quadrature, and is given in Eq.3.3 [4].

$$\sigma_t = \left(\sigma_f^2 + (1 + 1/64)\sigma_e^2\right)^{1/2}. \tag{3.3}$$

Additional sources of noise, not included in Eq. 3.3, may affect the measurement of hot electron temperature from the bremsstrahlung emission spectrum. These include counting x-rays that are reflected off the vacuum vessel walls or the the collimator into the field of view of the detector. Because it the LDX vacuum vessel is so large it was not possible to have each detector view a beam dump. Hard target bremsstrahlung

may also be a source of noise in the measurement.

DXP control software and driver

Two software packages are available from XIA to control the DXP. Mesa2X is a LabView program which allows the user to record and view spectra, baselines and statistics. A digital oscilloscope mode is available that shows the voltage trace of the preamplifier output and the outputs of the fast and slow filters. This program also includes an auto-calibration feature that calibrates the detectors to a single line source. Handel is a set of C libraries that provides the user with more flexibility than Mesa2X, but is not as automated. Mesa2X was used for testing and calibration, while the Handel libraries were integrated with the MDSplus data system and used for experimental runs.

Both programs required the development of a driver to be used with the LDX CAMAC hardware. The LDX is using a CAMAC 411s controller which interfaces between the computer and the CAMAC crate controller. MDSplus already includes a driver for the CAMAC 411s controller.

An interface has been written between the XIA Mesa2X and Handel programs and MDSplus[21], the data acquisition software used for the experiment. XIA software can now be operated with any hardware that has an MDSplus driver. The interface takes a command from Mesa2X and calls an MDSplus command on a user specified server from the remcam library which then executes the command using the built in driver. The camac controller is physically connected to the server which does not need to be the same computer that is running the Mesa2x software. The interface supports both VMS and Linux operating systems as the MDSplus server.

Using the Handel and MDSplus libraries, additional programs were written to control the initialization, triggering, and storage of data from the DXP into the MDSplus tree. These programs will operate the DXP in both single spectrum and time resolved mode.

Table 3.2: CZT detector gains in mV/keV calibrated using and iterated gaussian fit to the 59.5412 keV line of Am-241. Zero is measured as the offset of the baseline measurement.

Serial #	DXP Channel	Sensitivity [mV/keV]	Resolution [keV]
B1241	0	0.106486	2.05
B1242	1	0.102311	1.75
B1243	2	0.107559	1.85
B1244	3	0.103193	1.75

3.3 Calibration

The detectors were calibrated using an Am-241 source. The calibration line for this source is 59.5 keV[22]. The activity of the the source is such that count rates of 10^6 counts per second can be acheived. This is sufficient for testing pulse pileup characteristics. This line is in the low range of the LDX bremsstrahlung emission.

The detectors are calibrated using an iterated gaussian fit to the peak that is built in to the Mesa2X software. The time duration of each iteration is determined such that the height of the calibration peak is at least 1000 counts. Five iterations are used. The zero is set automatically in the software using the mean position of the baseline measurement.

The calibrated detector gain and baseline standard deviation for each channel are reported in Table 3.2. A typical Am-241 spectrum, as measured by CZT detector, B1242 is shown in Fig. 3-6. The variation in the baseline mean is generally less than 20 eV in the LDX configuration.

Before interacting with the detector, x-rays with the detector field of view must pass through a 0.005" beryllium vacuum window, 80–81 mm of air depending, and the detector windows, 0.001" Al. The x-ray signal is attenuated in each of these materials. The intensity, I transmitted through a foil is

$$I = I_0 \exp(-\mu x)$$

where I_0 is the incident intensity, μ is the material attenuation coefficient, and x is

the width of the foil. Each x-ray is transmitted or absorbed with probability, I/I_0. To calculate the number of x-rays produced from the number that are transmitted, is straightforward, $N_T = N * P(T)$. Transmission through each surface is independent, so the probability of transmission through all of the films is equal to the product of the probabilities of transmission through each surface.

$$\frac{I_n}{I_0} = \frac{I_1}{I_0}\frac{I_2}{I_1}...\frac{I_n}{I_n - 1} = exp(-\mu_1 x_1 - \mu_2 x_2 - ... - \mu_n x_n).$$

The detector response is corrected in the same way, except that the probability of absorption is used, rather than the probability of transmission. This method is valid in all regions where the attenuation coefficient is continuous. The only absorption resonance in the range of 10 keV to 1000 keV occurs for CZT at 31 keV.

The percentage probability of transmission through each foil and the total percentage of measuring a count are shown Fig. 3-8. The aluminum window on the CZT detector limits transmission at low energies. At energies above 130 keV, the probability of absorption by the CZT crystal limits the efficiency. Fig. 4-1 shows the raw counts per bin from the CZT detectors in black and counts per bin corrected for detector and window efficiency in blue.

Attenuation coefficients for air, beryllium and aluminum were obtain from the National Institute of Standards database[23], while attenuation coefficients for CZT were obtained from AmpTek products, a manufacturer of CZT detectors[24].

In addition to signal attenuation, the pulse height of an x-ray of a given energy is distorted by an effect known as 'hole tailing', in which spectral lines are observed with a tail of counts at lower energies [24]. This effect is property of the doped semiconductor so it applies to the CZT detectors, but not to the NaI detector. Electrons can become trapped in the holes in the semiconductor because the dimensions of the holes are smaller than the dimensions of the detector. As a result of this entrapment, the voltages produced by x-rays that react near the cathode of the detector are smaller than those that react near the anode. Pulses observed near the cathode have longer risetimes than pulse absorbed near the anode, so corrections for hole tailing are made

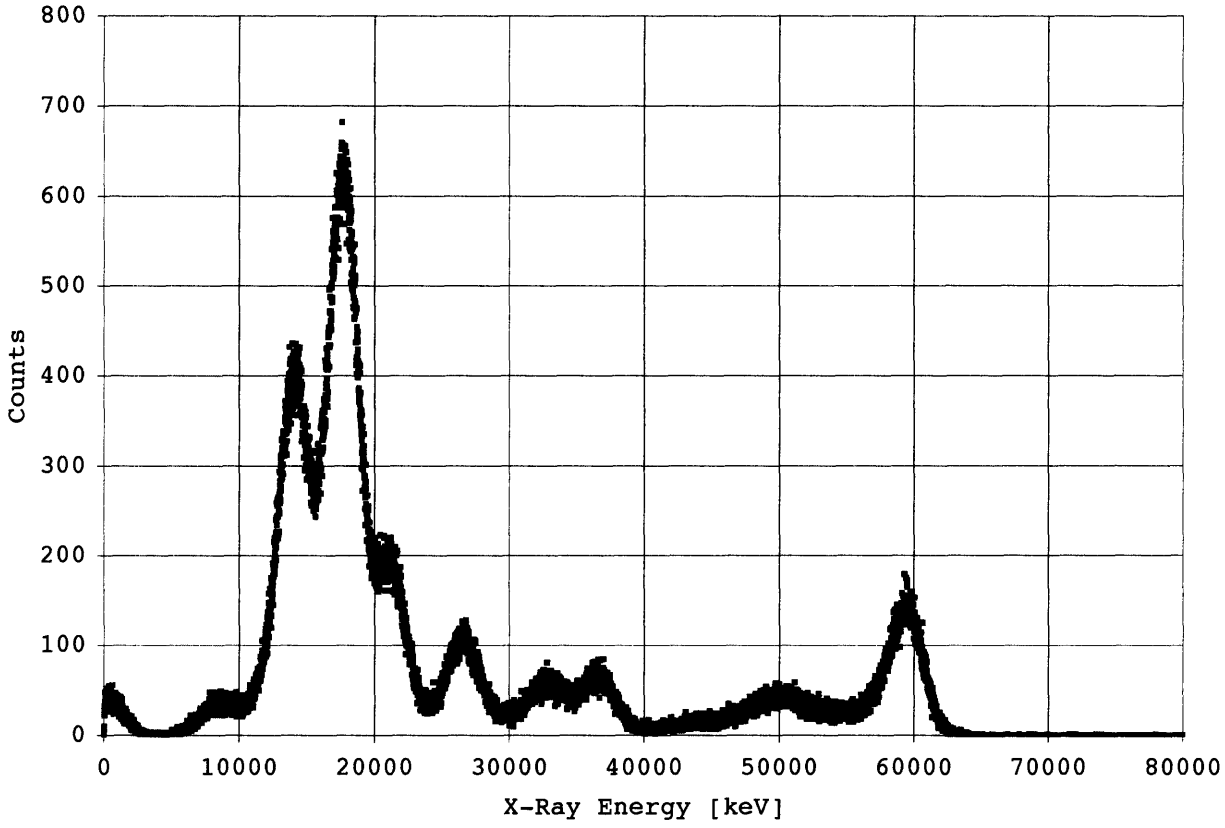

Figure 3-6: A typical Am-241 spectrum taken with a CZT detector using a threshold of 7 keV.

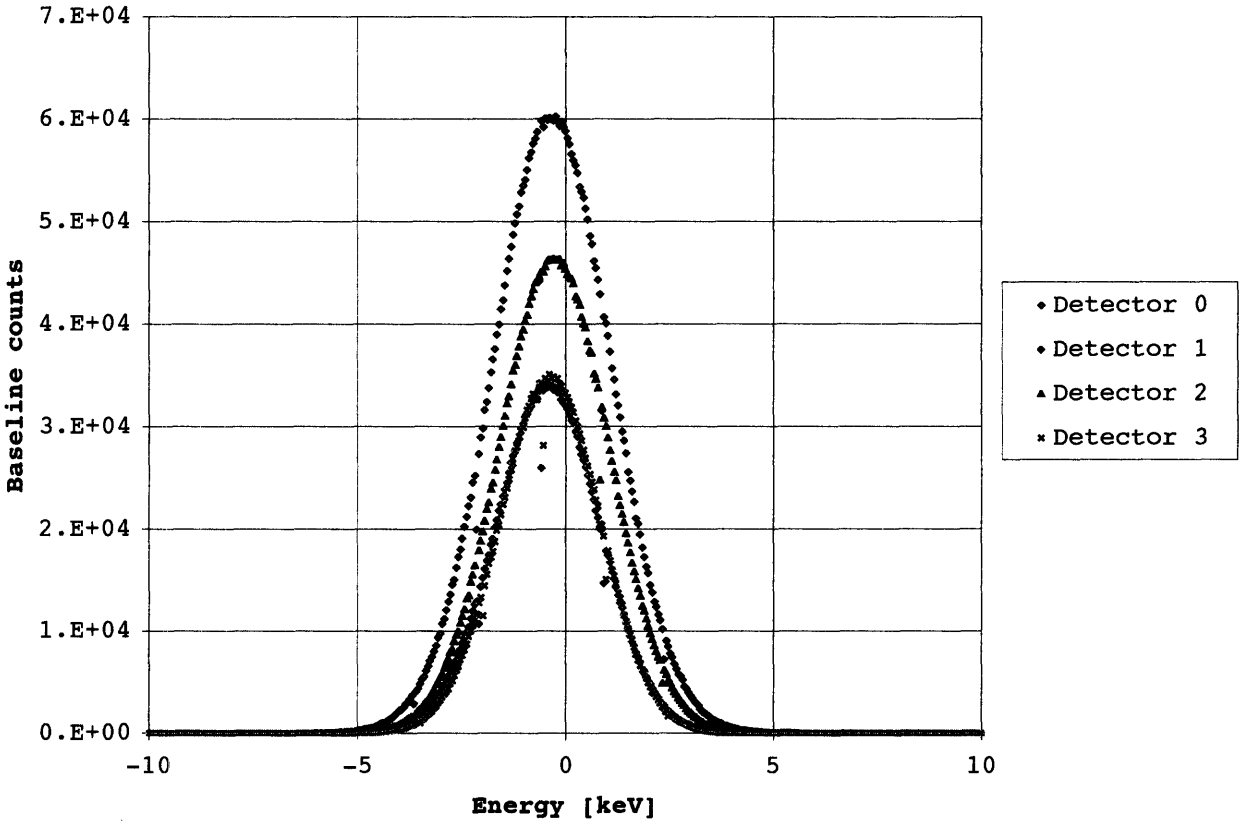

Figure 3-7: Typical baselines for CZT detectors are shown.

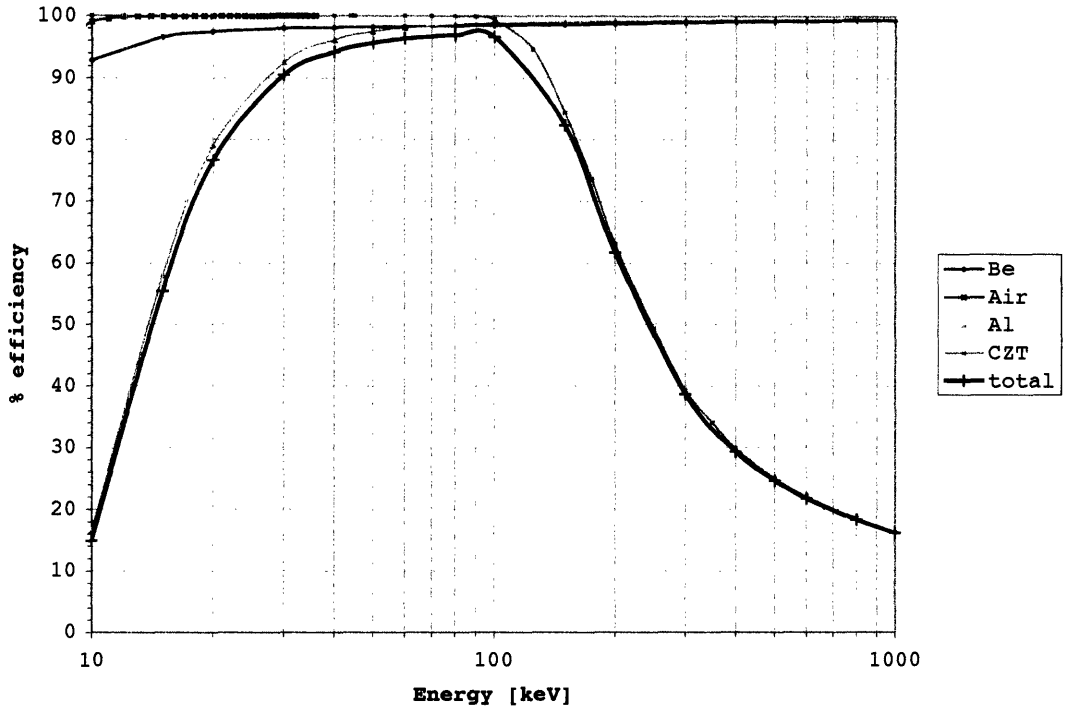

Figure 3-8: The percent efficiency of CZT detector, air and foils is shown versus energy in keV. These values were used to correct the raw data.

by rejecting pulses with long risetimes. The DXP requires the the pulse width be less than some maximum width, so the effects of hole tailing should be corrected by the DXP so long as the maximum pulse width is set to a small enough value.

Chapter 4

First Plasma Preliminary Results

First plasma experiments on LDX were conducted Friday, August 13, 2004. Two runs were conducted during which the F-coil was inductively charged to 750 kAmp–turns and lifted. The F-coil was then supported while deuterium plasmas were created in the surrounding space. The F-coil remained supported until it quenched, at which time it was lowered back into the charging station to be recooled. The F-coil was operated continuously for over 2 hours and 15 minutes during the second run, and for slightly less time during the first run.

These experiments utilized a single RF heating frequency, 6.4 GHz with 3 kW of power (the 2.45 GHz source described in earlier chapters didn't fire). RF power was not varied for these experiments. The heating times were varied from 1 s to 8 s. The base vacuum was in the low 10^{-7} Torr scale. A gas scan was conducted by varying the number of deuterium particles puffed into the vessel. The average vessel pressure during the shots ranged from from $1 * 10^{-5}$ to $4 * 10^{-5}$ torr.

Forty-nine shots were taken in total. Plasma was produced in forty-three of these shots. Shots taken in vacuum with gas puffing and RF were recorded as baseline measurments. X-ray measurements from the pulse height analyzer were obtained for forty-six shots. The three failures to record data occurred as a result of complications in integrating the DXP driver into the LDX data system. These integration issues can be resolved before the next set of runs. Overall the performance of the LDX and of the pulse height analyzer were a success.

4.1 X-Ray Spectra

The pulse height analyzer recorded the counts in each energy bin. The energy width of each of the 8192 bins was set to 100 eV for the first 16 shots, allowing a maximum energy of 819.2 keV to be recorded. This energy range covers the entire energy range of the CZT detectors. During these shots, the energies recorded ranged up to 200 keV so the energy per bin was reduced for subsequent shots to provide better energy resolution.

Channel zero views the plasma at an angle of 7.5 degrees and the subsequent channels view every ten degrees, up to 37.5 degrees for channel three. Electrons are heated at the position of the 6.4 GHz cyclotron resonance, so the pressure peak is expected to be in the vicinity of this resonance. Data confirms a larger x-ray flux on channels 0 and 1, which view the resonance region, than on 2 and 3 which view along chords further from the pressure peak. The detector collimation was adjusted for the the first 14 runs to provide maximum viewing area, which should maximize the counts per channel. After confirming that x-rays were being emitted from the plasma, the collimation angle was reduced for each channel to provide more spatial resolution. The viewing angle of the center of the detector was 6.0 degrees for channels 0 and 3, and 6.3 degrees for channel 1 and 2.

If the velocity distribution of the electrons is maxwellian, the hot electron temperature can be determined by fitting a straight line to the gradient of the intensity spectrum. During ECRH heating, it is unlikely that the velocity distribution of the hot electrons is maxwellian. Plasma afterglows are long enough that the electrons may equilibrate. Because the x-ray emission of the entire shot is measured, it is not possible to distinguish between these two regimes. We fit an effective temperature to the tail of the distribution in Fig. 4-2. The values were determined using a chi squared goodness of fit weighted by $\sqrt{N}$, the probabilistic error, to the data on a log-linear scale. The effective temperatures for channels 41 keV, 48 keV, 58 keV, and 59 keV for channels 0,1,2,3, respectively.

A notable feature of these spectra is the distinct peak present on channels 1,2,

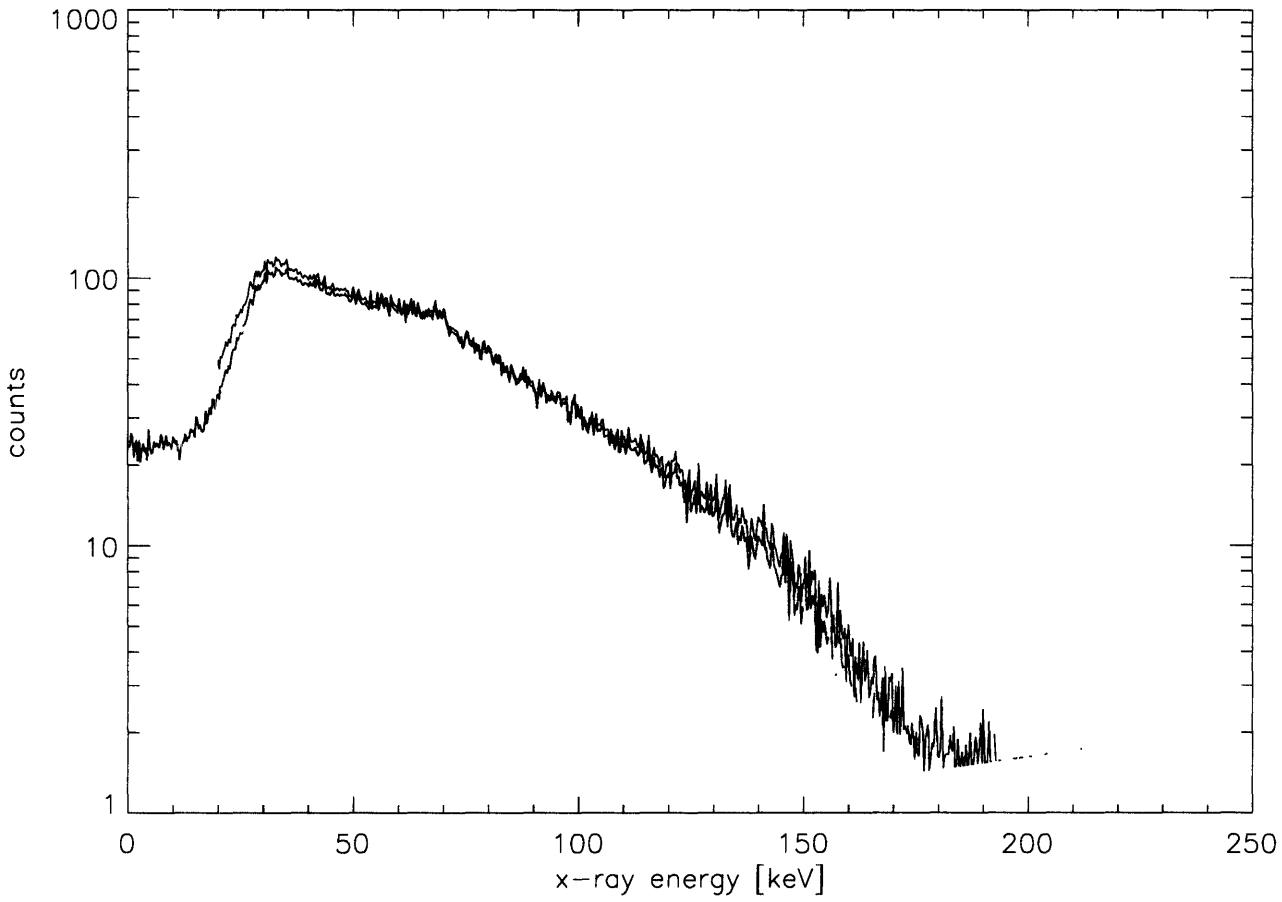

Figure 4-1: X-ray counts per energy bin for shot 40813020 as measured by the CZT detector for channel 0 detector are shown in blue. Data corrected for detector response and window losses are shown in black.

and 3. For shot 40813020, shown in Fig.4-2, the peak location is 89 keV. A peak is present on the spectra taken in many of the shots. The location of the peak varies from shot to shot as does it's intensity relative to the lowest energy maximum. Because the peak location varies, it is unlikely that this peak is due to impurity radiation. This peak may be due to hard target bremsstrahlung.

The temperatures fit to the distributions in channels 2 and 3 are larger than the temperatures on channels 0 and 1 which should view the plasma pressure peak. A possible explanation is that there is a mono-energetic distribution of hot electrons in the plasma with temperature of 89 keV. The error in the measurement of the location of the maximum counts is given by the width of the baseline, ± 2 keV. Further insight should be gained with time resolved measurements.

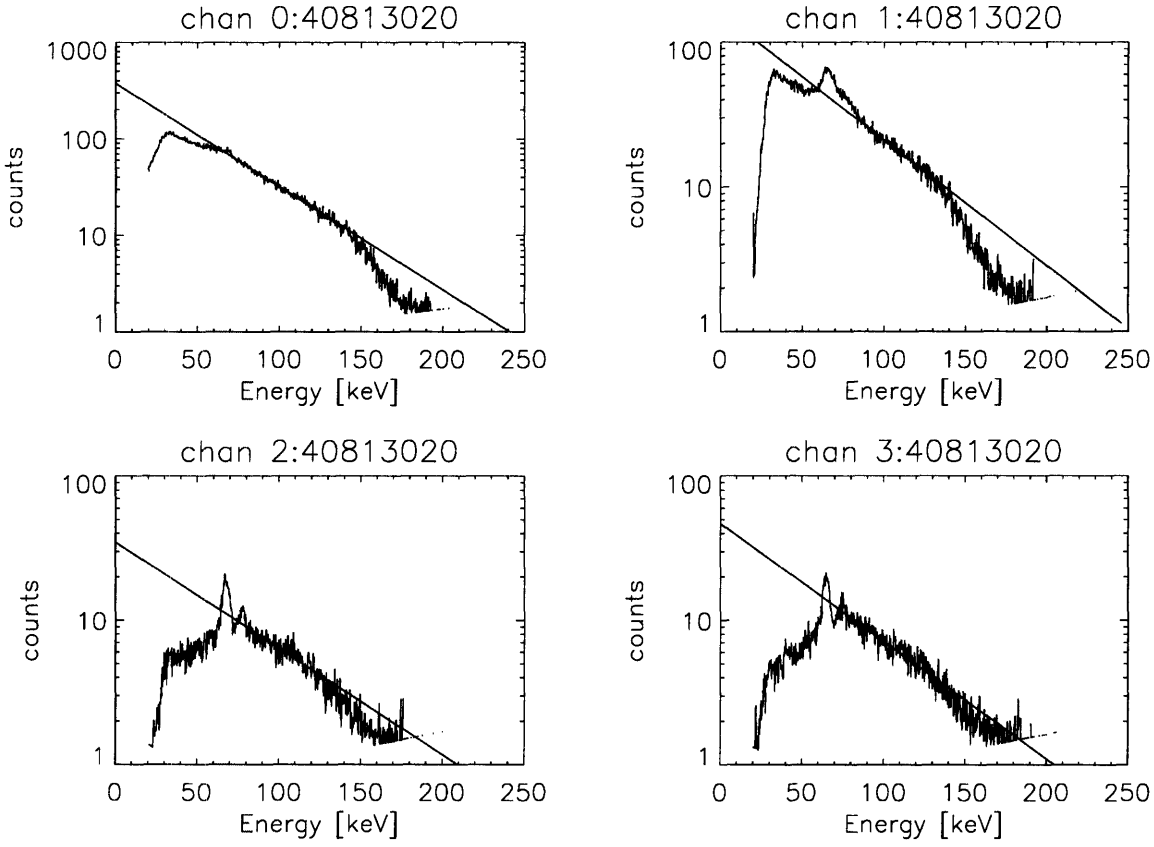

Figure 4-2: The number spectrum of x-ray emission, and a linear fit to the tail, are plotted versus energy for each of the four pulse height analyzer channels in shot 40813020. These spectra have been corrected for detector response and window losses.

4.2 Time Evolution of the Plasma

Video monitoring revealed bright plasmas that filled the vacuum vessel during the time when ECRH was applied. When the heating was turned off, a bright flash was followed by long lived, dim afterglows. Clips from a digital video of the plasma, taken at 16 frames per second are shown in Fig. 4-3. The times quoted are approximate as they were obtained by counting frames from the first frame where plasma was seen.

On some shots, bright flashes are observed near the inner support ring that holds up the F-coil, shortly after the ECRH is turned off. This flash was not observed in the video shown in Fig. 4-3, as the spike in visible light was not as intense as in other shots. A more intense event was observed in shot 40813020, see Fig. 4-4. The ECRH was turned off at 4.0012 seconds and it took approximately 3 ms for the ECRH forward power to fall to zero. The visible light emitted from the plasma begins to decrease at 4.0013 ms. This signal falls more slowly than the ECRH forward power. A small increase in x-ray intensity occurs between 4.01 and 4.012 seconds. At 4.01273 seconds, a the x-ray intensity spikes. A spike is observed on the reflected power measurement for the ECRH at 4.01274 seconds. at 4.01287 seconds, a spike is observed in the visible light and vacuum vessel pressure. This is the bright flash of light that was observed on the video. The time differences in the occurrence of these events may be due to drift between the digitizers.

The activity on the RF reflected power may indicate the presence of a microinstability with a frequency on the order of the 2.45 GHz cyclotron frequency. In this case, when the ECRH is turned off, the bulk plasma decays and the hot electrons in the plasma become unstable and diffuse into the loss cone. Alternatively, this may be caused by a hot electron interchange instability. The later pick up of visible light indicates the production of plasma due to to interactions between hot electrons and neutral particles. After the initial burst, slowly decaying afterglows are observed.

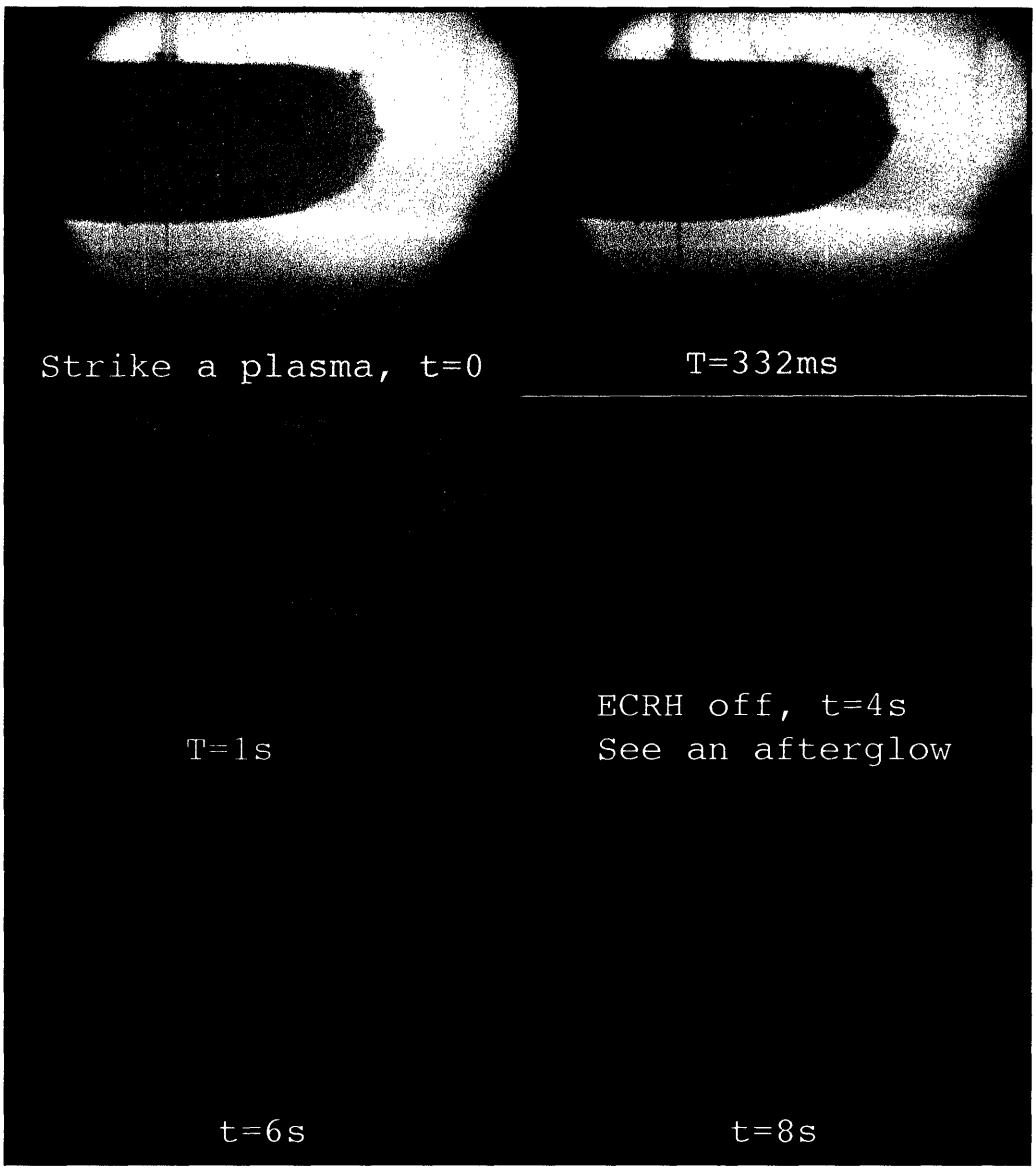

Figure 4-3: Six frames are shown from a video of shot 40813022. 6.4 GHz ECRH was turned on at t=0s and turned off at t=4 s.The afterglow was visible through t=12 s.

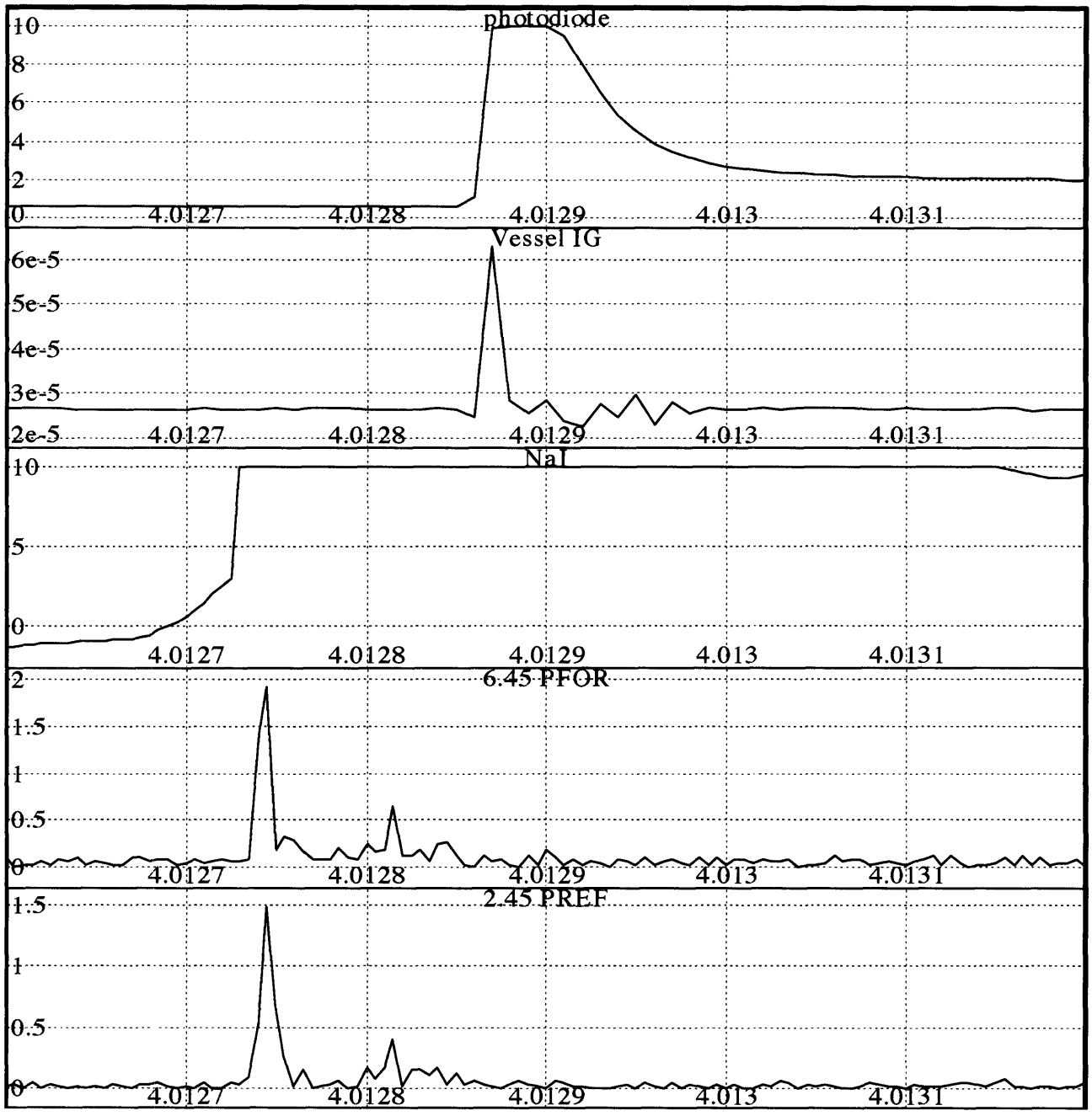

Figure 4-4: Photodiode signal, NaI detector signal ,Vacuum vessel pressure, 6.4 GHz ECRH forward power, 2.45 GHz reflected power,are shown versus time in seconds for shot 40813020. Except for pressure, all signals are in relative units.

4.3 Gas Puff Scan

A gas scan was conducted by varying the puff time while holding all other parameters constant. As expected, opening the puff valve for longer periods of time led to high pressures in the vessel. We would like to conduct experiments at the pressure which yields the most x-ray flux.

The total number of x-ray counts is plotted versus the vessel pressure for the puff scan in Fig. 4-5. The pressure values were adjusted to reflect the ion gauge calibration for deuterium gas, $P_{D2} = P_{N2}/0.35$. These values were used in the ideal gas law to determine the total number of particles injected into the vessel. The vacuum vessel volume is $40m^3$; room temperature, 297 K, was assumed. The x-ray flux is expected to decrease as the pressure in the vessel increases. For puff times of 60 ms and 100 ms, the total number of counts are less than those taken with shorter puff times.

The energy for these puff scan shots was estimated by fitting an exponential curve to the tail of the distribution for energy bins, in the region where the curve is roughly linear. Each spectra was considered individually. The data is rather flat. The total counts on channel 1show some increase in the area of 10^{20} particles injected.

4.4 Conclusions and Future Work

Time resolution is essential for proper diagnosis of LDX plasmas. The upgraded firmware for the DXP incorporating multi-mca mode must be integrated with the current system. In addition, improved filtering is necessary on the NaI x-ray intensity measurement. These systems will provide independent measurements of the temporal spectrum of x-ray emission from the plasma. In addition, work is ongoing to improve the integration of the DXP driver and the MDSplus data system. Appropriate functions will be written in the TDI programming language to upgrade the DXP from a node in the LDX tree to an MIT device. This will make it easier for users to operate the DXP.

As plasma heating and control improve, the x-ray flux is expected to increase.

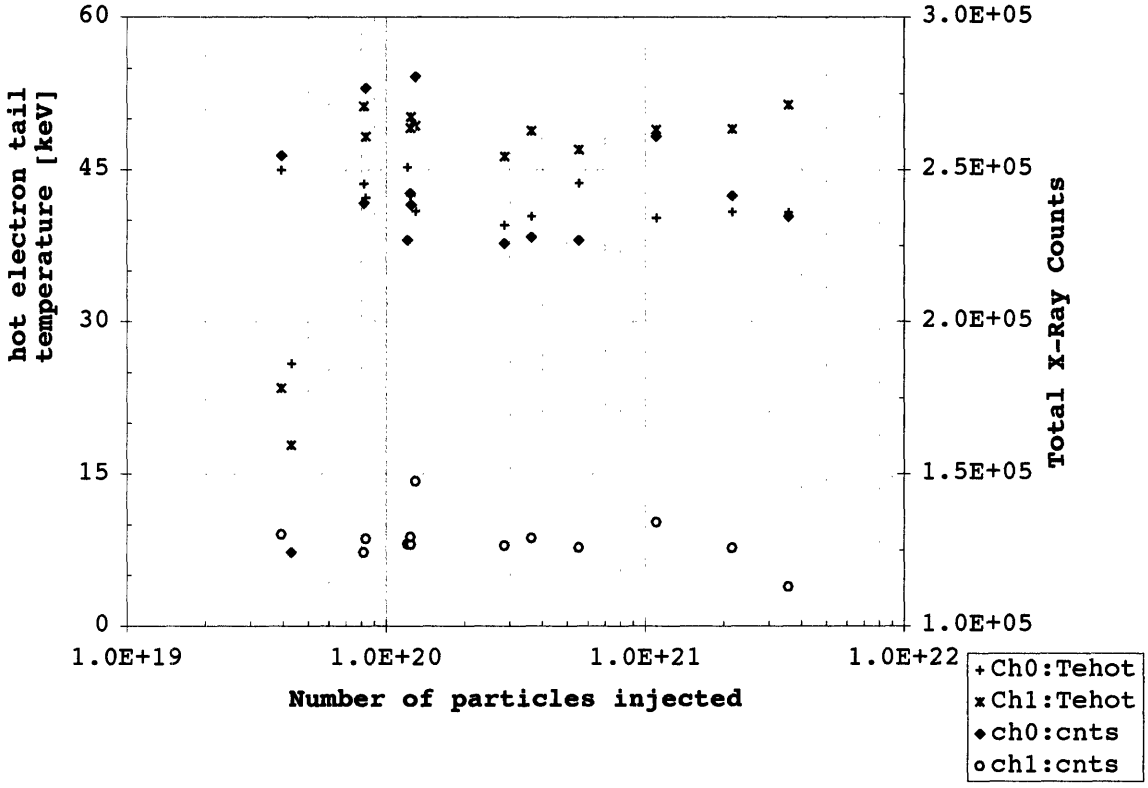

Figure 4-5: The hot electron temperature on the tail determined from an exponential fit to the x-ray emission is plotted on the left axis. The total number of x-ray counts per channel is plotted on the right. The number of deuterium particles puffed into the vessel is plotted on the independent axis

At this time it will be necessary to install a pinhole on the pulse height analyzer collimator to allow for improved spatial resolution in addition to shielding from hard target bremsstrahlung. At this time, an x-ray camera (Hamamatsu x-ray intensifier on loan from PPPL) will be installed on the LDX. The camera views x-rays with energies greater than 45 keV [25] The x-ray emission from the plasma is imaged onto a 25 mm diameter phosphor display. This image is filmed (in a light tight box) by a CCD camera with standard video output: 60 fields per second of 600x800 pixel images.

The x-ray pulse height analyzer was designed, installed, and tested on the LDX. Single spectra were obtained per shot. Peaks were observed on the x-ray spectra in the range of 60 keV - 90 keV. The source of these peaks is still under investigation, as is the unusual result that the temperatures observed on channels viewing the edge of the plasma are higher than those that view the peak of the plasma. The presence of a confinement degrading instability was observed during plasma afterglows.

Appendix A

Digital filter parameters chosen for LDX

The XIA digital x-ray processor (DXP) model 4C2X is used for the LDX pulse height analyzer. This system incorporates two fixed length, trapezoidal filters for pulse height determination and pile-up discrimination. The fast filter is used to determine the arrival time of the pulse and the pulse height, while the slow filter is used to improve energy resolution. Each filter has length, $2L + G$ where L is the time during which the filter voltage is increasing and G is the flat top time, as illustrated in Fig. A-1. The gap time should correspond to the rise time of the preamplifier voltage.

The slow filter should be chosen as short as possible to increase the throughput of the system which scales like $1/\tau_{ps}$, where τ_{ps} is the length of the slow filter, but long enough to achieve the desired energy resolution for the system. The fast filter should be chosen as long as possible to prevent fast pileup of pulses.

Table A.1 shows the filter characteristics used for initial plasma experiments. The filter parameters are input to the DXP in either clock units, 25 ns for a 40 MHz clock ($CLOCK_SPEED = 40$), or decimated clock units, $2^{DEC} * CLOCK\_SPEED$. The decimation, DEC can be 0,2,4,or 6 and is determined by the DXP based on the peaking time. The current LDX configuration uses a decimation of 2. The slow filters are measured in decimated clock units, while the fast filters are measured in clock units. SLOWLEN and FASTLEN are the lengths of the slow and fast trapezoidal filters,

respectively. Similarly, SLOWGAP and FASTGAP are the flattop times of the trapezoidal filters. PEAKINT is the peak interval time and is typically set to SLOWLEN + SLOWGAP. PEAKSAM is the time at which the pulse height is sampled. This parameter can vary from SLOWLEN to PEAKINT-1. This parameter should be set such that the maximum count rate is achieved. A scan of the parameter using the LDX setup with CZT detectors found that value of PEAKINT - 4 yielded the maximum count rates, but there was very little difference in the count rates when values from PEAKINT-3 to PEAKINT-5 were used. THRESHOLD is the threshold for the fast filter trigger. Pulses smaller than the threshold are not measured.

Table A.1: Filter parameters chosen for initial plasma runs on LDX.

Filter Parameter	Value	Time
SLOWLEN	12	1.2 μs
SLOWGAP	6	600 ns
FASTLEN	5	125 ns
FASTGAP	1	25 ns
PEAKINT	18	1.8 μs
PEAKSAM	13	1.3 μs
MINWIDTH	2	200 ns
MAXWIDTH	20	2 μs
THRESHOLD	64	15 keV

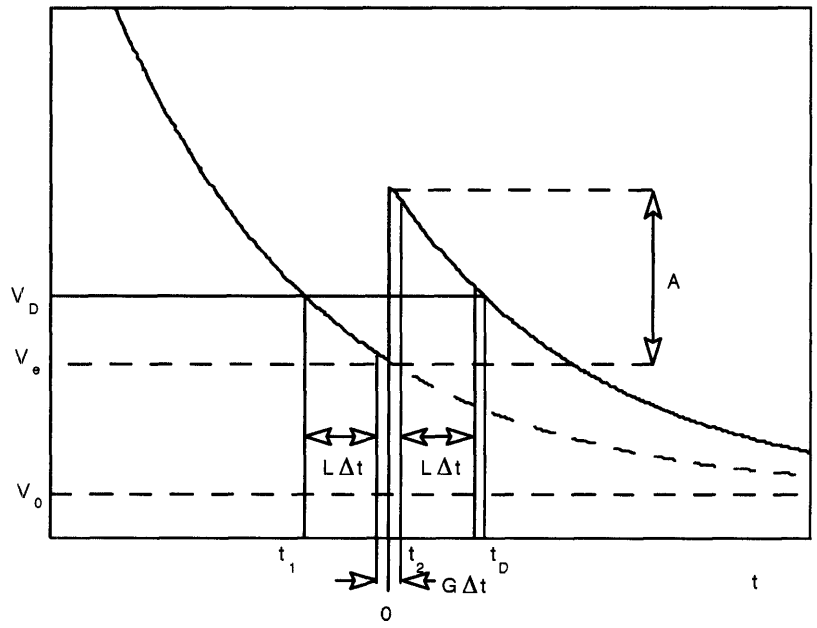

Figure A-1: Illustration of the filter parameters, length, L and gap, G for the DXP. Reproduced with permission from XIA [4].

Bibliography

[1] J. Kesner and M. Mauel. Levitated dipole experiment. `http://www.psfc.mit.edu/ldx/reports/LDX_2003.pdf`, April 2003.

[2] 2004. Figure provided by A.K. Hansen.

[3] D.T. Garnier et.al. Overview and experimental prograam of the levitated dipole experiment. In *presented at 45th Annual Meeting of the American Physical Society Division of Plasma Physics*, October 2003.

[4] X-Ray Instrumentation Associates, Newark, CA. *Users Manual: Digital X-Ray Processor Model DXP2X*, a edition, June 2002.

[5] M.J. Kilveson and C.T. Russel, editors. *Introduction to Space Physics.* Cambridge University Press, 1st edition, 1995.

[6] A. Hasegawa Cont Fus. A dipole field fusion reactor. *Comm Pl Phys & Cont Fus*, 11(3):147, 1 1987.

[7] J. Kesner, L. Bromberg, D.T. Garnier, and Mauel M.E. Plasma confinement in a levitated dipole. In *presented at 17th IAEA Conference of Plasma Physics and Controlled Nuclear Fusion*, pages IAEA–F1–CN–69/IC, Yokohama, Japan, 1998.

[8] J. Kesner, L. Bromberg, M. Mauel, D. T. Garnier, and J.M. Dawson. The dipole fusion confinement concept: A white paper for the fusion community. Technical Report PSFC/RR-98-5, MIT Plasma Science and Fusion Center, April 1998. Accessed 20 Aug. 2004.

[9] J. Kesner, D.T. Garnier, A. Hansen, M. Mauel, and L. Bromberg. D–d fusion in a levitated dipole. *Nuclear Fusion*, 44:193, 2004.

[10] D. T. Garnier, J. Kesner, and M. E. Mauel. Ecrh on the levitated dipole experiment. In *presented at 13th Topical Conference on Applications of Radio Frequency Power to Plasmas*, Annapolis, MD, April 1999.

[11] J. Kesner and D. T. Garnier. Convective cell formation in levitated dipole. *Phys. Plasmas*, 7:2733, 2000.

[12] I. H. Hutchinson. Chapter 5.3: Radiation from electron-ion encounters. In *Principles of Plasma Diagnostics*, pages 186–214, Cambridge, 2002. Cambridge University Press.

[13] J. Sinnis, M. Okabayashi, J. Schmidt, and S. Yoshikawa. Particle loss in the levitated spherator fm-1. *Phys. Rev. Lett.*, 29(29):1214–1218, 1972.

[14] D.M. Meade and W.E. Wilson. *Bull. Am. Phys. Soc.*, 9:532, 1964.

[15] A.C. Riviere and D.R. Sweetman. The culham superconducting levitron. In *5th European Conference on Controlled Fusion and Plasma Physics*, volume 2, page 95, 1972.

[16] H.P. Warren and M.E. Mauel. Observation of chaotic particle transport induced by drift–resonant fluctuations in a magnetic dipole field. *Phys. Rev. Lett.*, 74(8):1351, February 1994.

[17] J. Kesner and R.J. Hastie. Electrostatic drift modes in a close field line configuration. *Phys. Plasmas*, 9(2):396, 2001.

[18] Saint-Gobain Crystal & Detectors. X-ray probes and detectors. `http://www.bicron.com/xray.htm`. Accessed 25 Aug. 2002.

[19] eV Products. Spear detector datasheet.

[20] M.E. Mauel. personal communication.

[21] T.W. Fredian and J.A. Sillerman. X-windows-based user interface for data acquisition and display. *Rev. Sci. Instrum.*, 61(10):2383, 2990.

[22] Y. A. Akovali. Www table of radioactive isotopes. `http://ie.lbl.gov/education/isotopes.htm`. Accessed 8 Aug 2004.

[23] J.H. Hubbell and S.M. Selzer. Tables of x-ray mass attenuation coefficients and mass energy-absorption coefficients. `http://physics.nist.gov/PhysRefData/XrayMassCoef/cover.html`. Accessed 21 Aug. 2004.

[24] Bob Redus. Czt efficiency application note. Technical Report ANCZT-1 Rev.1, AmpTek, 2001.

[25] S. von Goeler, S. Jones, R. Kaita, S. Bernabei, W. Davis, H. Fishman, G. Gettelfinger, D. Ignat, F. Paoletti, G. Petravich, F. Rimini, P. Roney, J. Stevens, and W. Stodiek. Camera for imaging hard x rays from suprathermal electrons during lower hybrid current drive on pbx-m. *Rev. Sci. Instrum.*, 65:1621, May 1994.